Available online at www.sciencedirect.com

ScienceDirect

Advances in Space Research 76 (2025) 7351–7374

ADVANCES IN SPACE RESEARCH (a COSPAR publication)

www.elsevier.com/locate/asr

Ionospheric response to superstorm in May 2024 over mid- and high-latitude Eurasia

M.A. Chernigovskaya [a,*], G.A. Zherebtsov [a], K.G. Ratovsky [a], A.G. Setov [a], D.S. Khabituev [a], A.S. Kalishin [b], S.A. Dolgacheva [b], A.E. Stepanov [c], A.Yu. Belinskaya [d], V.V. Bychkov [e], S.A. Grigorieva [f], V.A. Panchenko [g], A.V. Timchenko [h]

[a] *Institute of Solar-Terrestrial Physics SB RAS, Irkutsk, Russia*
[b] *Arctic and Antarctic Research Institute, St.Petersburg, Russia*
[c] *Institute of Cosmophysical Research and Aeronomy SB RAS, Yakutsk, Russia*
[d] *Trofimuk Institute of Petroleum Geology and Geophysics SB RAS, Novosibirsk, Russia*
[e] *Institute of Cosmophysical Researches and Radio Wave Propagation of the FEB RAS, Paratunka, Russia*
[f] *Institute of Geophysics UB RAS, Ekaterinburg, Russia*
[g] *Pushkov Institute of Terrestrial Magnetizm Ionosphere and Radio Wave Propagation RAS, Moscow, Russia*
[h] *Pushkov Institute of Terrestrial Magnetism, Ionosphere and Radio Wave Propagation (Western Branch) RAS, Kaliningrad, Russia*

Received 21 July 2025; received in revised form 24 September 2025; accepted 26 September 2025
Available online 30 September 2025

Abstract

The spatio-temporal variations in ionospheric, geomagnetic and atmospheric parameters over Eurasia were studied based on data obtained during the extreme magnetic storm in May 2024 from high- and mid-latitude chains of ionosondes and magnetometers belonging to INTERMAGNET and Russian observatories. Analysis of the F2-region critical frequencies and their relative deviations from the mean (based on ionosonde measurement data), and the standard deviations of the components of the surface main geomagnetic field (GMF) (based on magnetometer measurement data) enabled us to distinguish strong latitudinal and longitudinal differences in specific features of variations in geophysical parameters, both under quiet conditions before the magnetic storm onset and during the storm. With the onset of the magnetic storm, variability of GMF components was more pronounced in midlatitudes and increased by an order of magnitude: from 80 to 800 nT for H-component, and from 60 to 600 nT for Z-component. Longitudinal distribution of GMF variations clearly distinguishes longitudes with maximum and minimum intensity of variations. Almost immediately after the storm began at 17:00 UT on 10 May 2024, according to measurements from all ionosondes, a drop in electron concentration was detected at the height of F2-layer maximum regardless of the measurement point local time. During the storm's main phase (late 10 May and early 11 May 2024) until the evening of 12 May 2024, total radio blackouts exceeding one-and-a-half days occurred at every high-latitude ionosonde. Thus, strong effects of a negative ionospheric storm were noted in both high- and mid-latitude regions during the main and early recovery phases of the magnetic storm. Additional bursts of geomagnetic activity in the storm's recovery phase in certain time intervals on 11–13 May 2024 were also followed by significant and long-lasting decreases in electron concentration. At high latitudes, there was a radio blackout for several hours during the transition from 12 to 13 May 2024. From the second half of May 13, the electron concentration began to increase to the pre-storm level, which continued until May 14–15 at all longitudes of the mid- and high-latitude region of Eurasia. At the end of the magnetic storm recovery phase, from the second half of day on 14 May and 15 May 2024, a so-called aftereffect of geomagnetic storm (time interval of increased electron concentration) was observed according to the data the mid- and high-latitude ionosondes over Eurasia. The fact of observing this phenomenon in the high latitude region is unusual and very remarkable. Also, a very interesting fact is that longitudinal regions with strong negative variations for 10–12 May 2024 match those with enhanced variations in GMF components during the magnetic storm. A long-term negative disturbance of electron concentration covering a huge ter-

* Corresponding author.
E-mail address: cher@iszf.irk.ru (M.A. Chernigovskaya).

https://doi.org/10.1016/j.asr.2025.09.082

ritory of mid-latitude Eurasia, was induced by an extraordinary, catastrophic drop in the density ratio [O]/[N_2] according to GUVI TIMED satellite measurements during the superstorm for almost three days.

Keywords: Ionosonde chains; Chains of magnetometers; Ionospheric disturbances; Geomagnetic field variations; Geomagnetic storm

1. Introduction

The paper presents the results of a study on the ionospheric effects of the most powerful geomagnetic disturbance of the current solar cycle 25 and of the current century, which occurred on 10–15 May 2024.

In general, throughout the history of observations, the strongest magnetic storm occurred on 2 September 1859 (the Carrington Event) with estimated Dst ranging from −850 to −1760 nT. The most intensive geomagnetic storm of the 20th century occurred on 13–15 May 1921 (estimated Dst = −907 ± 132 nT). Such low Dst-indices make these two events the largest in the modern age.

After calculations of Dst-index began in 1957 (Sugiura and Kamei, 1991), the strongest geomagnetic disturbance occurred on 13 March 1989 (Quebec Event), when Dst = −589 nT. Between 1957 and the end of the 20th century, only three magnetic storms exhibited similar levels of minimum Dst-index, specifically those taking place on 13 September 1957, 11 February 1958, and 15–16 July 1959. The 11 February 1958 geomagnetic storm, which was followed by famous midlatitude planetary aurora, showed the minimum Dst of −426 nT.

The strongest magnetic storms of the 21st century were observed on 29–31 October.

(Dst = −401 nT) and 20 November (Dst = −472 nT) 2003. These were G5 superstorms, also known as the Halloween storms (Gopalswamy et al., 2005).

Thus, the magnetic storm in May 2024 was one of the strongest throughout the history of observations. This highly intensive geomagnetic event undoubtedly raised great interest among researchers involved with atmosphere–ionosphere-magnetosphere couplings. The anticipated practical consequences of the strongest magnetic disturbance affecting Earth may include various issues, such as: disruptions in reliable radio and cell phone communications, malfunctions in navigation and positioning systems (e.g., impaired operation of GPS and HF communication systems can lead to disorientation of ships, aircraft, etc.), and failures in operation of power systems. Space forecast services sent preliminary reports and notifications about the likely geomagnetic disturbance of maximum intensity to allow for preventive measures.

According to estimates in (Øvstedal, 2002), a one-unit change in total electron content (TEC) can cause an error of up to 0.16 m in positioning with a single-frequency GPS receiver, which most civil users employ for navigation purposes. Thus, severe TEC variations during magnetic storms can lead to significant positioning/navigation errors with single-frequency GPS receivers. During this storm, a considerable worsening of GPS positioning accuracy was also registered (Tulasi et al., 2024).

The group of infrastructural elements subject to influence by geomagnetic storms includes pipelines, railways, and power lines. Various-purpose space satellites face exposure to high-energy particles originating from the solar wind and radiation, both of which negatively affect onboard equipment and crew life-support systems. One recent example is the G2 moderate magnetic storm that occurred on 2–3 February 2022. After this storm, 40 of the 49 Starlink satellites launched a few days earlier were actually factually disabled (Berger et al., 2023).

The first and most visible manifestation of the magnetic disturbance's effect on Earth was the widespread observation of numerous auroras during this event. Data collected using both professional scientific instruments and ordinary smartphones/cameras by millions of observers proved invaluable for characterizing this extraordinary natural phenomenon. In addition, because the event occurred near the summer solstice in the Northern Hemisphere, many optical instruments were unable to operate due to the absence of appropriate dark conditions (Grandin et al., 2024; Hayakawa et al., 2024). Cumulative reports were received from nearly seven hundred citizen scientists in over 30 countries. Based on the analysis of data collected, it was concluded that the aurora was visible in regions with geomagnetic latitudes ranging from 30° to 60° N GMlat (Grandin et al., 2024). Several reports were also received from lower latitudes. This was significantly closer to the equator than predicted by auroral oval models. As reported by participants, the prevailing red and pink colors of the observed auroras were intense enough to be visible to the naked eye. The authors of (Hayakawa et al., 2024) collected amateur records of observed auroras during the May 2024 superstorm. They used these records to reconstruct the equatorial boundary of the visual auroral oval, which reached a magnetic latitude of 23.2° S GMlat (Namibia). Based on historical naked-eye observations, this storm was similar to the Great Storms that occurred on 11 February 1958 (the minimum Dst of −426 nT), which was followed by the famous planetary midlatitude aurora, and on 15–16 July 1959, for which the auroral oval equatorial boundary was reconstructed until |23,3|° and |27,4|° GMlat, respectively (Hayakawa et al., 2024).

This strong equatorward extension of the auroral region observed by many indirectly indicates an equally essential shift of the subauroral ionospheric region adjoining the auroral oval toward lower latitudes – a transition from high to middle latitudes. A typical large-scale spatial feature of the subauroral ionosphere structure is the main ionospheric trough (MIT) of ionization. The minimum of MIT is located not more than 5° equatorward of the auroral oval boundary (Rodger et al., 1992; Aladjev et al., 2001; Deminov and Shubin, 2018; Karpachev, 2021).

In addition to practical effects of top-level geomagnetic disturbances on living conditions and health, events of this class are of great scientific interest. During magnetic storms, a series of complex processes – ionospheric storms (negative and positive when the electron concentration is decreased/increased, respectively) develop in the ionosphere, resulting in significant changes in ionospheric parameters (Matsushita, 1959; Prölss, 1995; Rishbeth, 1998; Buonsanto, 1999; Mikhailov, 2000; Danilov, 2013). First of all, disturbances in the Earth's ionosphere are induced by a sequence of interrelated events that begin with manifestations of enhanced solar activity. These events later affect the solar wind — magnetosphere — ionosphere system. In other cases, ionospheric disturbances may be caused by internal factors within the ionosphere — thermosphere system connected to processes in the neutral atmosphere. In both cases, ionospheric ionization disturbances of various intensities occur, leading to ionospheric inhomogeneities of different spatial and temporal scales. Development of negative or positive ionospheric storm phase depends greatly on the local time, season, and geographical region (Prölss, 1995; Rishbeth, 1998; Buonsanto, 1999; Mendillo, 2006; Burešová et al., 2007; Ratovsky et al., 2020).

At previous stages of our studies, which were based on data from Eurasian mid- and high-latitude ionosondes, GPS/GLONASS receivers, and INTERMAGNET magnetometers, we considered spatio-temporal features of ionospheric response over the mid- and high-latitude Eurasia during extreme magnetic storms in March and June 2015 (Chernigovskaya et al., 2021; Chernigovskaya et al., 2024a, b), and long-term series of magnetic storm in March 2012 (Chernigovskaya et al., 2023). The patterns of the ionospheric response to geomagnetic disturbances differ and are related to the seasonal probability of a positive or negative phase of an ionospheric storm. Comprehensive studies conducted during magnetic storms using radiophysical sounding techniques revealed significant latitudinal and longitudinal variations in ionospheric parameters. We concluded that the revealed longitudinal variations in ionospheric parameters are caused by longitudinal features of the main geomagnetic field (GMF) structure and its variations in response to changes in geomagnetic conditions. Additionally, we found that the magnetic and geographical poles do not align (so-called UT-variations). In the course of research, attention was focused on the existing problem of disturbances in parameters of the ionospheric F2-layer occurring before the onset of geomagnetic storms, known as pre-storm disturbances (Burešová and Laštovička, 2007; Danilov and Konstantinova, 2019; Ratovsky et al., 2020). An important result of previous studies is the conclusion that the ionospheric effects of strong magnetic storms should be considered on a timescale of several days after the main phase of the magnetic storm and even after the end of its recovery phase. This is due to the fact that the disturbed active regions of thermospheric gas continue to move westward by inertia and induce variations in electron concentration along the propagation trajectory. For instance, low ionization was observed during the recovery phase (2–4 days after the main phase) of extreme magnetic storm in March 2015 (Chernigovskaya et al., 2021; Chernigovskaya et al., 2024a, b), and a series of magnetic storms in March 2012 (Chernigovskaya et al., 2023). Another interesting effect of ionospheric response to magnetic storms is its "final chord" in a sequence of complicated atmospheric-ionospheric interaction processes. This effect, known as an ionospheric aftereffect, occurs when the ionosphere recovers after a magnetic storm at middle latitudes. During this time, electron densities can exceed values observed on quiet days prior to the onset of a magnetic disturbance (Namgaladze et al., 1988; Klimenko et al., 2018; Ratovsky et al., 2018). (Chernigovskaya et al., 2021; Chernigovskaya et al., 2024a, b) noted that over Eurasian longitudes, the negative phase of the ionospheric storm during both the main and recovery phases of the March 2015 magnetic storm transitioned into a positive phase following the end of the geomagnetic disturbance.

In this paper, we continue our research through a comprehensive analysis of the spatial and temporal features of ionospheric inhomogeneities over Eurasia. This analysis is based on ionosonde measurements of an extraordinary magnetic storm event in May 2024, for which we use the methods developed earlier.

2. Experimental data

To analyze spatio-temporal variations in ionospheric parameters during the May 2024 extreme geomagnetic disturbance, we use data on the hourly average (or hourly – for ionosondes in Novosibirsk and Kaliningrad) values of the F2-layer critical frequency – foF2 as measured by the Eurasian chains of mid- and high-latitude ionosondes. The high-latitude chain comprises 6 ionosondes located at 67°–71° N (geomagnetic latitudes 58°<GMlat < 64° N) in the 26°–129° E longitude sector of the Eurasian continent (Fig. 1a, red marks; Table 1). This chain includes ionosondes that belong to Russian research organizations: ISTP SB RAS and IKFIA SB RAS – DPS-4 at Norilsk and Zhigansk stations (Reinisch et al., 1997) and AARI of Roshydromet – CADI (MacDougall et al., 1995; Vystavnoi et al., 2013; Kalishin et al., 2020) at Lovozero, Salekhard, and Tiksi stations. Also, we use data from

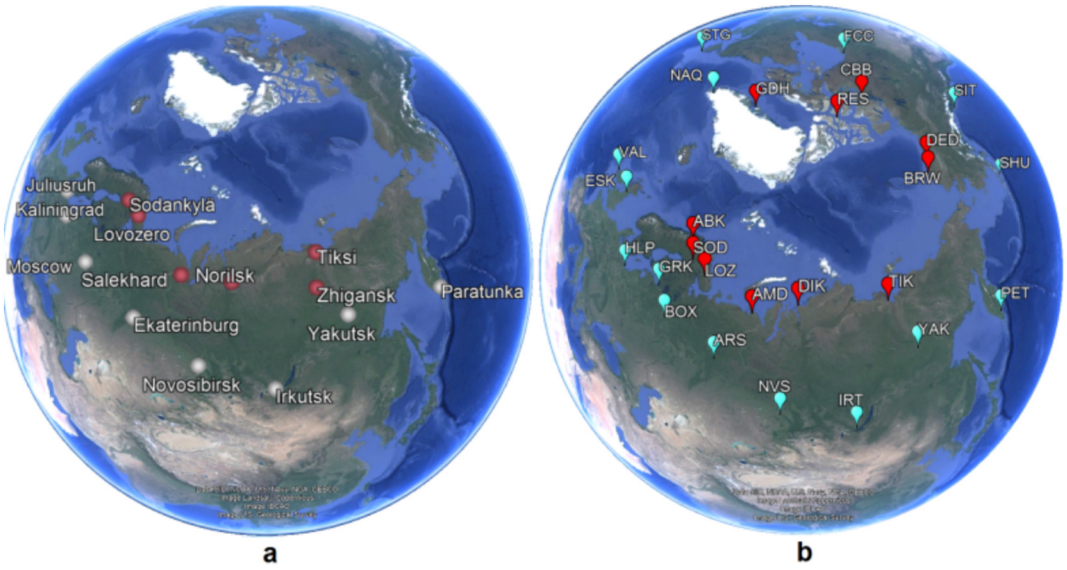

Fig. 1. Maps of ionosonde (a) and magnetometer (b) chain positions.

Table 1
High-latitude ionosondes.

Ionosonde	Ionosonde	Geographical coordinates		Geomagnetic coordinates	
		Latitude	Longitude	Latitude	Longitude
Sodankylä (SOD)	SO166	67° N	26° E	64° N	118° E
Lovozero (LOV)	CADI	68° N	35° E	64° N	126° E
Salekhard (SAH)	CADI	67° N	67° E	59° N	150° E
Norilsk (NOR)	DPS-4	69° N	88° E	60° N	166° E
Zhigansk (ZHG)	DPS-4	67° N	123° E	58° N	168° W
Tiksi (TIK)	CADI	71° N	129° E	63° N	165° W

SO166 ionosonde (Alpha Wolf) in Sodankylä Geophysical Observatory in Finland (Enell et al., 2016).

The mid-latitude chain comprises 8 ionosondes located at 52°–62° N (geomagnetic latitudes 42°<GMlat < 54° N) in the 13°–158° E longitude sector (Fig. 1a, white marks; Table 2). The chain comprises 4 digital ionosondes DPS-4 of different modifications (IKFIA SB RAS, Yakutsk; ISTP SB RAS, Irkutsk; IZMIRAN, Moscow; the Leibniz Institute of Atmospheric Physics, Juliusruh, Germany) (Reinisch et al., 1997), 3 Russian ionosondes "Parus" of different modifications (IKIR FEB RAS, Paratunka; IGF UB RAS, Ekaterinburg; WB IZMIRAN, Kaliningrad) (Krasheninnikov et al., 2010) and "Ionosonde-MS" in IGG SB RAS, Novosibirsk (Podlesnyi et al., 2013).

As agreed by the study participants, all ionograms were processed manually to minimize errors that could occur in

Table 2
Mid-latitude ionosondes.

Ionosonde	Ionosonde	Geographical coordinates		Geomagnetic coordinates	
		Latitude	Longitude	Latitude	Longitude
Juliusruh (JUL)	DPS-4D	55° N	13° E	54° N	99° E
Kaliningrad (KGD)	Parus A	55° N	21° E	53° N	106° E
Moscow (MSK)	DPS-4	56° N	37° E	52° N	122° E
Ekaterinburg (EKB)	Parus 3.0	57° N	60° E	50° N	141° E
Novosibirsk (NVS)	Ionosonde-MS	55° N	83° E	50° N	160° E
Irkutsk (IRK)	DPS-4	52° N	104° E	42° N	177° E
Yakutsk (YAK)	DPS-4	62° N	130° E	53° N	163° W
Paratunka (PAR)	Parus 2.0	53° N	158° E	46° N	138° W

automated processing. The ionosonde measurement data from Juliusruh (https://giro.uml.edu/didbase/scaled.php) and Sodankylä (https://www.sgo.fi/Data/Ionosonde/ionData.php) taken from the websites are presented in automatic processing without manual verification.

Time resolution of the analyzed experimental data varies depending on the ionosonde. It ranges from 15 min (ionosondes in Paratunka, Yakutsk, Zhigansk, Irkutsk, Norilsk, Ekaterinburg, Moscow, Juliusruh, Sodankylä), 30 min (ionosondes in Tiksi, Salekhard, Lovozero) to 1 h (ionosondes in Novosibirsk and Kaliningrad). To fill the gaps in the ionosonde data time series when constructing spatio-temporal distributions, we used the triangulation method with linear interpolation of neighboring available measurements. During the considered magnetic storm period from 9 to 15 May 2024, there were periods without measurement data due to technical issues in Ekaterinburg (from 14:00 UT on 11 May to 2:30 UT on 12 May 2024; from 9:45 UT on 13 May to 8:15 UT on 14 May 2024); Salekhard (from 11:00 to 13:00 UT on 15 May 2024); Zhigansk – until 12 May 2024. Operation of DPS-4 ionosonde in Yakutsk was extremely unstable, so the measurement data is very fragmentary.

As in previous studies based on measurement data from the mid- and high-latitude ionosonde chains (Chernigovskaya et al., 2021; Chernigovskaya et al., 2024a, b), we used the F2-layer critical frequency foF2 to examine the magnetic storm effects in maximum electron concentration variations. The critical frequency is related to the F-region maximum electron concentration by formula $NmF2\ (m^{-3}) = 1.24 \times 10^{10} \times (foF2(MHz))^2$ (Polyakov et al., 1968).

To reconstruct spatial structure and temporal variations in geomagnetic field, we used data from INTERMAGNET (https://www.intermagnet.org) and from mid- and high-latitude Russian observatories: Tiksi, Dikson, Amderma, Lovozero, Gorkovskaya – Geophysical Department of AARI (https://aari.ru/departments/geophys); Borok – obs. Borok, Schmidt Institute of the Physics of the Earth (IPE) RAS (https://geodata.borok.ru/database/magnetic-field/index); Arti – obs. Arti of IGF UB RAS (https://igfuroran.ru/ob-institute/struktura/observatoriya-arti/); Yakutsk – obs. Yakutsk of IKFIA SB RAS (https://ikfia.ysn.ru/data/lmii/intermagnet). The stations for geomagnetic observations were divided into two chains (Fig. 1b): high-latitude – along ~70° N (11 magnetometers shown as red circles) and mid-latitude – along ~55° N (15 magnetometers shown as blue circles). Table 3 contains stations' coordinates and IAGA codes.

According to the method developed in (Shpynev et al., 2018), we used hourly standard deviations (mean square deviations or MSD) of the GMF horizontal H- and vertical Z-components relative to the corresponding background undisturbed values as the main characteristic of GMF variability for each observation point. The use of MSD as a statistical assessment of GMF components' variability during geomagnetic disturbances allows us to avoid the potential influence of differences in the analyzed initial data on components of the Earth's magnetic field associated with magnetometer modifications (Fig. 2b, Table 3). Background values of GMF components were calculated as a running mean over ± 14 days for each hour, based on data collected during magnetically quiet days preceding the geomagnetic storm onset. This averaging excludes the influence of solar and lunar tides in diurnal variations. Time series of MSD values, calculated for each station in the high- and mid-latitude magnetometer chains for the analyzed time interval of the storm, were employed to plot longitude-temporal maps of variations in the GMF components H and Z under quiet and disturbed geomagnetic conditions.

Table 3
High-latitude and mid-latitude magnetometers of the Northern Hemisphere.

No.	Station	IAGA codes	Geographical coordinates	
			Latitude	Longitude
High-latitudes ~70° N				
1	Abisko	ABK	68.4	18.8
2	Sodankylä	SOD	67.4	26.6
3	Lovozero	LOZ	68.0	35.0
4	Amderma	AMD	69.5	61.4
5	Dixon	DIK	73.5	80.6
6	Tiksi Bay	TIK	71.6	129.0
7	Barrow	BRW	71.3	203.4
8	Deadhorse	DED	70.4	211.2
9	Cambridge Bay	CBB	69.1	255.0
10	Resolute Bay	RES	74.7	265.1
11	Kekertarsuak	GDH	69.3	306.5
Mid-latitudes ~55° N				
1	Hale	HLP	54.6	18.8
2	Gorkovskaya	GRK	60.1	29.2
3	Borok	BOX	58.1	38.2
4	Arti	ARS	59.4	58.6
5	Novosibirsk	NVS	54.8	83.2
6	Irkutsk	IRT	52.2	104.5
7	Yakutsk	YAK	62.0	129.7
8	Paratunka	PET	53.0	158.2
9	Shumagin Island	SHU	55.4	199.6
10	Sitka	SIT	57.1	224.7
11	Fort Churchill	FCC	58.8	265.9
12	St. John's	STJ	47.6	307.3
13	Narsarsuaq	NAQ	61.2	314.6
14	Valentia	VAL	51.9	349.8
15	Escdalemur	ESK	55.3	356.8

To analyze spatio-temporal variations in neutral gas composition in the ionosphere, satellite measurements of atmospheric gas column $[O]/[N_2]$ were used for heights above ~100 km within the thermosphere (ionosphere), obtained with the GUVI TIMED UV-spectrometer using the optical method.

3. Characteristics of May 2024 magnetic storm

The cause of the strongest geomagnetic disturbance of the current century, which occurred on 10–15 May 2024,

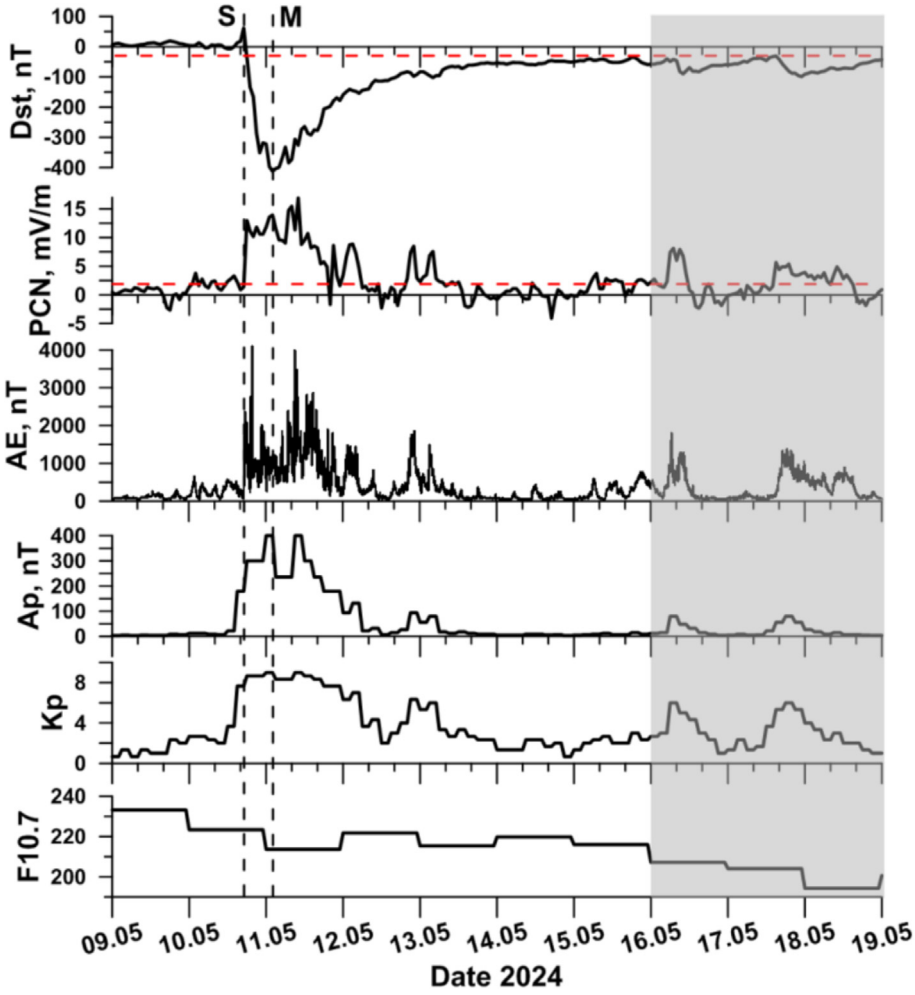

Fig. 2. Variations in geomagnetic and solar activity indices. The storm threshold levels of Dst and PCN values are shown by red horizontal dashed lines. Vertical dashed lines show the time of the storm onset (labeled S) and the timepoint of the magnetic storm maximum intensity (labeled M).

was the enhanced solar activity after a long period of low solar activity. In the interval from 8 through 11 May 2024, several powerful solar flares occurred in active region 3664 (8 May 2024 – a X1.0 flare and several M flares; 9 May – X2.25 and X1.12 flares; 10 May – a X3.98 flare; 11 May at 01:23 UTC – another X flare of 5.4–5.7 magnitude) (SWPC PRF 2541, 13.05.2024). At least seven coronal mass ejections (CMEs) related to the above solar flares and directed toward Earth (SWPC PRF 2541, 13.05.2024), reached the planet on 10 to 12 May 2024, and produced the strongest long-lasting geomagnetic storm. The passage of the interplanetary shock wave was observed on 10 May 2024 at 16:39 UTC. For the rest of the day on 10 May, the Bz-component of the interplanetary magnetic field (IMF) remained directed southward, decreasing to −50 nT at times. With the shockwave arrival, the solar wind velocity increased from 450 km/s to 700 km/s, and reached its peak of approximately 1000 km/s at 00:57 UTC on 12 May (SWPC PRF 2541, 13.05.2024).

Fig. 2 shows temporal variations in geomagnetic and solar activity indices during the development of the analyzed magnetic storm. The magnetic storm commenced in the evening of 10 May 2024 at 17:00 UT (SSC time – Sudden Storm Commencement – is shown as a vertical dashed line labeled S). By 21:00 UT, the geomagnetic disturbance intensity reached an extreme level (from −200 to −350 nT) and the G4 category (Kp = 8) (see Dst and Kp graphs in Fig. 2). One hour later, by 22:00 UT on 10 May, the intensity reached the "great storm, or superstorm" class (Dst-index lower than −350 nT) according to storm classification by planetary Dst (Loewe and Prölss, 1997) and the extreme G5 category according to NASA's classification based on the Kp index (https://www.swpc.noaa.gov/noaa-scales-explanation). After midnight on 10–11 May, the magnetic storm intensified to its maximum level. At 02:00 UT, Dst decreased to −412 nT (shown in Fig. 2 as the vertical dashed line labeled M), and Kp reached a value of 9 according to data from the World Data Center for Geomagnetism, Kyoto (https://wdc.kugi.kyoto-u.ac.jp/wdc/Sec3.html). The storm main phase lasted for ~9 h. At the storm maximum, Ap index grew up to 400 nT (https://wdc.kugi.kyoto-u.ac.jp/wdc/Sec3.html).

In this work, we analyze the helio-geomagnetic effects on the mid- and high-latitude ionosphere. In addition to geomagnetic indices Dst, Kp and Ap, we employ geomagnetic activity indices AE (Auroral Electrojet) and PCN (Polar Cap North) that describe magnetic activity in the polar caps (Fig. 2). AE describes magnetic disturbance induced by enhanced currents in the ionosphere, specifically the eastern and western polar electrojets, which flow along the auroral oval boundary. The unified PC index describes the magnitude of geoeffective interplanetary electric field that impacts the magnetosphere, as well as the dynamic pressure of the solar wind (Troshichev and Sormakov, 2018).

Noteworthy is a significant AE increase up to 4098 nT at 19:48 UT (data from the AARI Geophysical Department, St. Petersburg) and PCN — up to 13–14 mV/m almost immediately after the SSC event with further growth up to 14 mV/m at the time of the storm maximum (data from the WDC for STP, Moscow – World Data Center for Solar Terrestrial Physics — https://www.wdcb.ru/stp/geomag/geomagn_PC_ind.ru.html) (Fig. 2). A significant PCN increase indicates strengthening of solar wind drivers of the storm (Troshichev and Sormakov, 2018; Kalishin et al., 2020). The strong correlation between the PCN and AE enhancements evidences that the interplanetary electric field and solar wind dynamic pressure had a highly geoeffective impact on the magnetosphere and ionosphere in the Earth's polar region. This resulted in a significant strengthening of currents along the auroral oval boundary in the ionosphere – the eastern polar electric jet (AE > 0).

Additional bursts of geomagnetic activity were observed in the storm recovery phase – at 9:00–10:00 UT on 11 May, and during transitions from 11 to 12 May and from 12 to 13 May. These enhancements of geomagnetic disturbance are clearly seen through variations in PCN, AE, Ap and Kp, and are undoubtedly connected to arrivals of CMEs reaching Earth after solar flares on 9, 10, and 11 May 2024 (SWPC PRF 2541, 13.05.2024). No intensification was noted in Dst variations during these periods. This may be due to propagation geometry of solar wind fluxes. After 9 May (SWPC PRF 2541, 13.05.2024), the rotation of active region 3664 out of alignment with the Sun-Earth line directed new coronal mass ejections offside from Earth, causing them to graze the Earth's magnetosphere tangentially.

The solar activity index F10.7 – the F10.7 flux of radio emission of 10.7 cm wavelength (2800 MHz) – varied from 233 s.f.u. on 9 May 2024 to 216 s.f.u. on 15 May 2024 (1 s.f.u. (solar flux unit) = 10^{-22} Watts m^{-2} Hz^{-1}) (https://www.wdcb.ru/stp/data/solar.act/flux10.7/daily/). This corresponds to the solar activity growth phase in current solar cycle 25 with its maximum predicted for 2025–2026.

Horizontal red dashed lines in Fig. 2 show the storm threshold levels of Dst = −30 nT (Loewe and Prölss, 1997) and PCN of ~2 mV/m (Troshichev and Sormakov, 2018). These levels indicate that the superstorm recovery phase continued for almost 5 days until 15 May 2024 (inclusively). On 16 and 17 May, there occurred new G2 moderate geomagnetic storms (shown with gray fill in Fig. 2), therefore, we considered the time interval until 15 May 2024, as it refers to the spoken geomagnetic disturbance.

Fig. 3 presents longitude-temporal distributions of standard deviations of the GMF H- and Z-components in the Northern Hemisphere, as measured by magnetometer chains that belong to INTERMAGNET and Russian observatories at high (panels a, b) and middle (panels c, d) latitudes. Additionally, to reconstruct the GMF spatial structure and temporal variations under quiet and disturbed conditions, we analyzed longitudinal distributions of standard deviations of the GMF H- and Z-components in polar coordinates for certain moments on geomagnetically quiet day on 9 May 2024 before the magnetic storm began (left columns in Figs. 3b, d) and on disturbed days 10–11 May 2024 during the superstorm main phase (right columns in Figs. 3b, d) at high- ~70° N (Fig. 3b) and mid-latitudes ~55° N (Fig. 3d). The grey dashed lines (radii) on the maps in polar coordinates show the geographic longitudes of the location of the high- (Fig. 3b) and mid-latitude (Fig. 3d) chains magnetometers (Fig. 1b; Table 3).

Geomagnetic activity is known to enhance during magnetic storms due to sharp changes in the existing current systems in the Earth's magnetosphere and ionosphere, or due to the formation of new current systems. Powerful corpuscular fluxes impacting the magnetosphere cause it to compress, and surface currents along the magnetospheric boundary to enhance. During the magnetic storm main phase, when the IMF Bz-component becomes directed southward, disturbed electric fields are generated (Tsurutani et al., 2004; Huang, 2013): 1) almost immediately occurring zonal prompt penetration electric fields (PPEFs) often seen at equatorial latitudes, and 2) delayed ionospheric electric fields generated by disturbed dynamo driven by Joule heating due to storm energy input at high latitudes –disturbance dynamo electric fields (DDEFs). This results in a significant increase in GMF strength during the initial and main phases of a magnetic storm, especially the horizontal H-component of the Earth's magnetic field.

Under quiet conditions before the storm began, the GMF variability was stronger at high- than at mid-latitudes (left columns in Figs. 3b, d). With the onset of the magnetic storm, variability of the GMF components was more pronounced in midlatitudes and increased by an order of magnitude: from 80 to 800 nT for H-component (Fig. 3d, top distributions) and from 60 to 600 nT for Z-component (Fig. 3d, bottom distributions). Considering the fact that in general, the GMF strength varies within 25,000–65,000 nT, these variations do not exceed few percent. But even GMF-component variations of this order evidence that the magnetic storm was highly geoeffective.

It's evident that longitudinal inhomogeneities of GMF variations are most pronounced during powerful geomag-

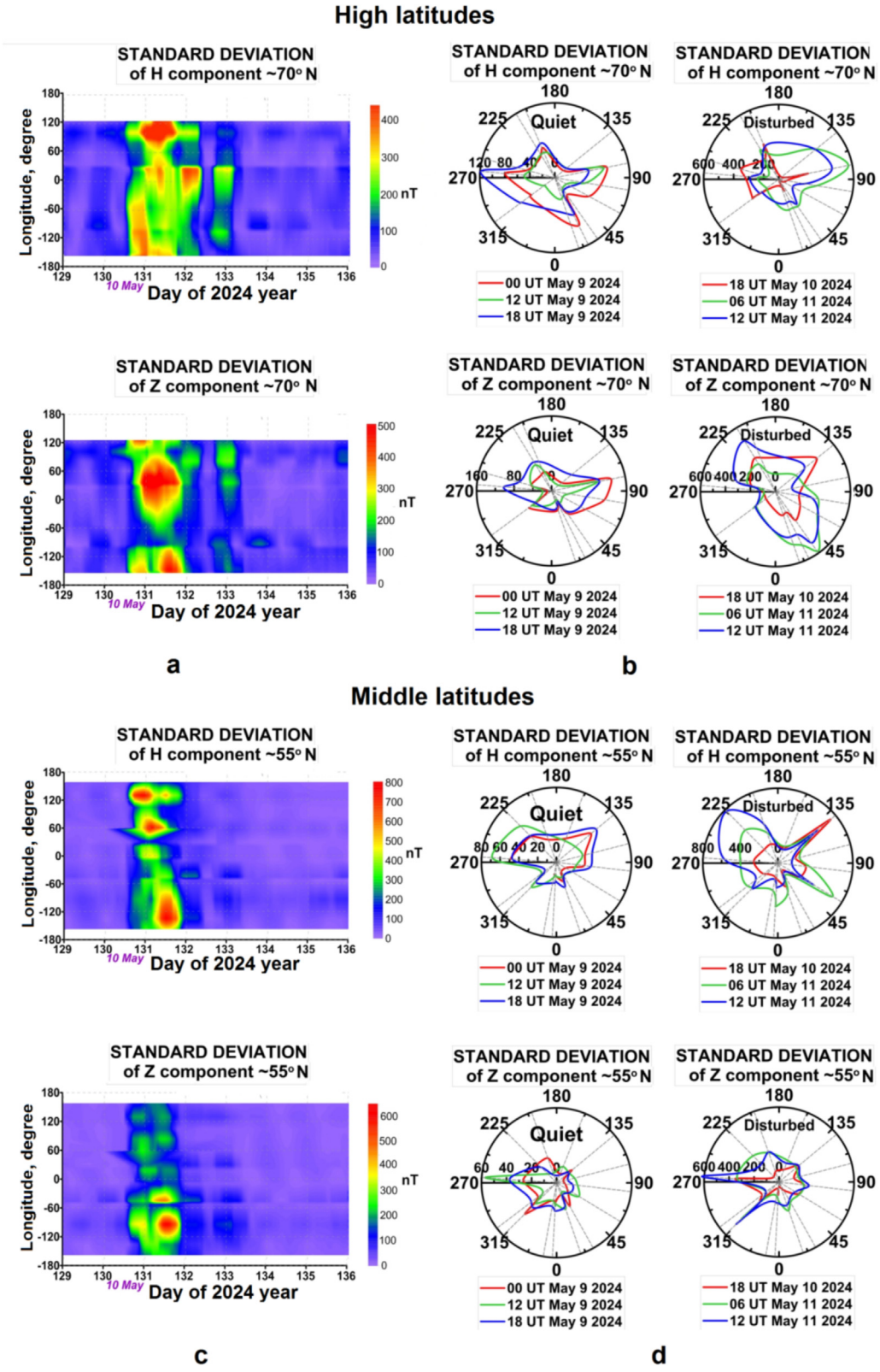

Fig. 3. Longitude-temporal variations in standard deviations of *H*- and *Z*-components on 9–15 May 2024 (UT) at high- ~70° N (a) and mid-latitudes ~55° N (c) and distributions of GMF standard deviations in polar coordinates for certain days in May 2024 for quiet (left column) and disturbed conditions (right column) at high- ~70° N (b) and mid-latitudes ~55° N (d). Lables on horizontal axes of polar coordinate distributions (b and d) are standard deviations of the GMF *H*- and *Z*-components in nT.

netic disturbances when distinct longitudinal sectors characterized by elevated GMF variations form, lacking longitudinal symmetry. As in our previous studies of magnetic storm events in March 2015, June 2015, and March 2012 (Shpynev et al., 2018; Chernigovskaya et al., 2021; Chernigovskaya et al., 2023), the longitudes where the intensity of variations has maxima and minima are clearly distinguishable in the longitudinal distribution of GMF variations (Fig. 3). In most cases, the maximum variability of standard deviations of the GMF H- and Z-components is observed at mid-latitudes (near ~55° N) (Fig. 3c). At high-latitudes (near ~70° N), the GMF variability is more uniform in longitude (Fig. 3a), but longitudinal inhomogeneities in GMF variations are also evident. The authors consider the revealed longitudinal structure of the GMF variability in quiet geomagnetic conditions is caused by the discrepancy of the geographic and magnetic poles (the UT effect) and by the spatial anomalies of different scales in the main magnetic field of the Earth. In mid-latitudes, one could see the significantly enhanced GMF variations for over a day starting from the storm onset on the evening of 10 May until the end of 11 May (Fig. 3c), i.e. throughout the storm main phase and in early recovery phase of the storm. In high-latitudes, intense GMF variations lasted even longer – from the storm onset to the middle of 12 May 2024. The main GMF disturbance during the storm main phase almost merged with the additional burst of geomagnetic disturbance during the transition from 11 to 12 May. After a certain weakening, the GMF disturbance intensified again at the change-over from 12 to 13 May (UT,) when another burst of geomagnetic disturbance arrived at Earth (Fig. 2). Additional bursts of geomagnetic disturbance can also be seen via longitude and time variations in GMF components at mid-latitudes (Fig. 3c), though the magnitude of these deviations is considerably lower than at high-latitudes (Fig. 3a).

Under geomagnetically disturbed conditions, longitudinal asymmetry of GMF variations is particularly pronounced, especially for horizontal GMF H-component at midlatitudes (Fig. 3d). Over Eurasia, two zones with the maximum GMF variations are distinguished at longitudes of ~40°–50° and ~130°–135°. Over the North-American sector, there are three active zones at ~225°, ~270° (near the geomagnetic pole longitude) and ~315° longitude. In the sector near the geomagnetic pole longitude, the GMF variations are significant, which is quite natural due to high magnetic latitude. We interpret these longitude sectors as the regions, where disturbances from the high-latitude ionosphere maximally penetrated into midlatitudes. The same longitudinal regions of intense GMF variations were mentioned earlier, when investigating into the ionospheric effects of a number of magnetic storms in solar cycle 24 in March 2015, June 2015 (Shpynev et al., 2018; Chernigovskaya et al., 2021) and March 2012 (Chernigovskaya et al., 2023). Normally, these longitudes of the Northern Hemisphere exhibit strong negative ionospheric disturbances during magnetic storms, i.e. decreased foF2 compared to undisturbed conditions, which is associated with low electron concentration in the F2-layer maximum. Analysis of measurement data from a magnetometer chain revealed the same longitudes of enhanced GMF variations at midlatitudes for the magnetic storm event in May 2024.

Over Eurasia, between zones with maximal GMF variations at ~40° and ~130° longitude, above the region of the East-Siberian positive continental magnetic anomaly located at ~80°–110° longitudes, GMF variability at middle latitudes is typically minimal (Figs. 3c, d).

At high latitudes (near ~70° N), GMF variability is more uniform in longitude (Fig. 3b), but longitudinal inhomogeneities in GMF variations are also evident.

Similar patterns of manifestations of longitudinal inhomogeneity in GMF component variations (petal-shaped structures of longitudinal variations in polar coordinates) for the mid-latitude region of the Northern Hemisphere under geomagnetically disturbed conditions were also distinct during magnetic storm events in March 2015, June 2015. (Shpynev et al., 2018; Chernigovskaya et al., 2021), and March 2012 (Chernigovskaya et al., 2023).

4. Data analysis and discussion: foF2 longitude-temporal variations in the mid- and high-latitude ionosphere over Eurasia

Top panels in Figs. 4a, b show longitude-temporal variations in critical frequency foF2 of the ionosphere, as measured by Eurasian ionosonde chains at middle (Fig. 4a) and high latitudes (Fig. 4b) for 9–15 May 2024. Middle panels in Figs. 4c, d show variations in dfoF2(t) of current foF2(t) from the background level expressed in fractions of one unit. Background values were calculated by averaging experimental measurements of foF2(t) using a 27–day running mean over the smoothing interval of (t–14, t + 14) days before and after each current hour t of a day. Then, we used time series of initial hourly data foF2(t) to calculate series of deviations from the background level. Analysis of relative deviations in the F2-layer's critical frequency provides a clear measure of how much impact a storm-related geomagnetic disturbance has compared to the undisturbed electron concentration conditions on quiet days before the onset of a geomagnetic disturbance (the SSC time is shown as vertical dashed lines on distribution maps and labeled S on the graph of Dst variations, see Fig. 4e). In addition, this analysis eliminates potential ambiguity in determining the ionospheric parameter on different types of ionosondes. Black horizontal dashed lines on the maps in Fig. 4a–d show longitudes where the high- (Fig. 1a; Table 1) and mid-latitude (Fig. 1a; Table 2) ionosonde chains are located, extending from west to east (bottom to top, respectively). Gray rectangles indicate periods with no data available due to technical issues or blackouts of ionosonde radio signals.

Bottom panels in Fig. 4e show storm-time variations in Dst and PCN. Red horizontal dashed lines depict storm

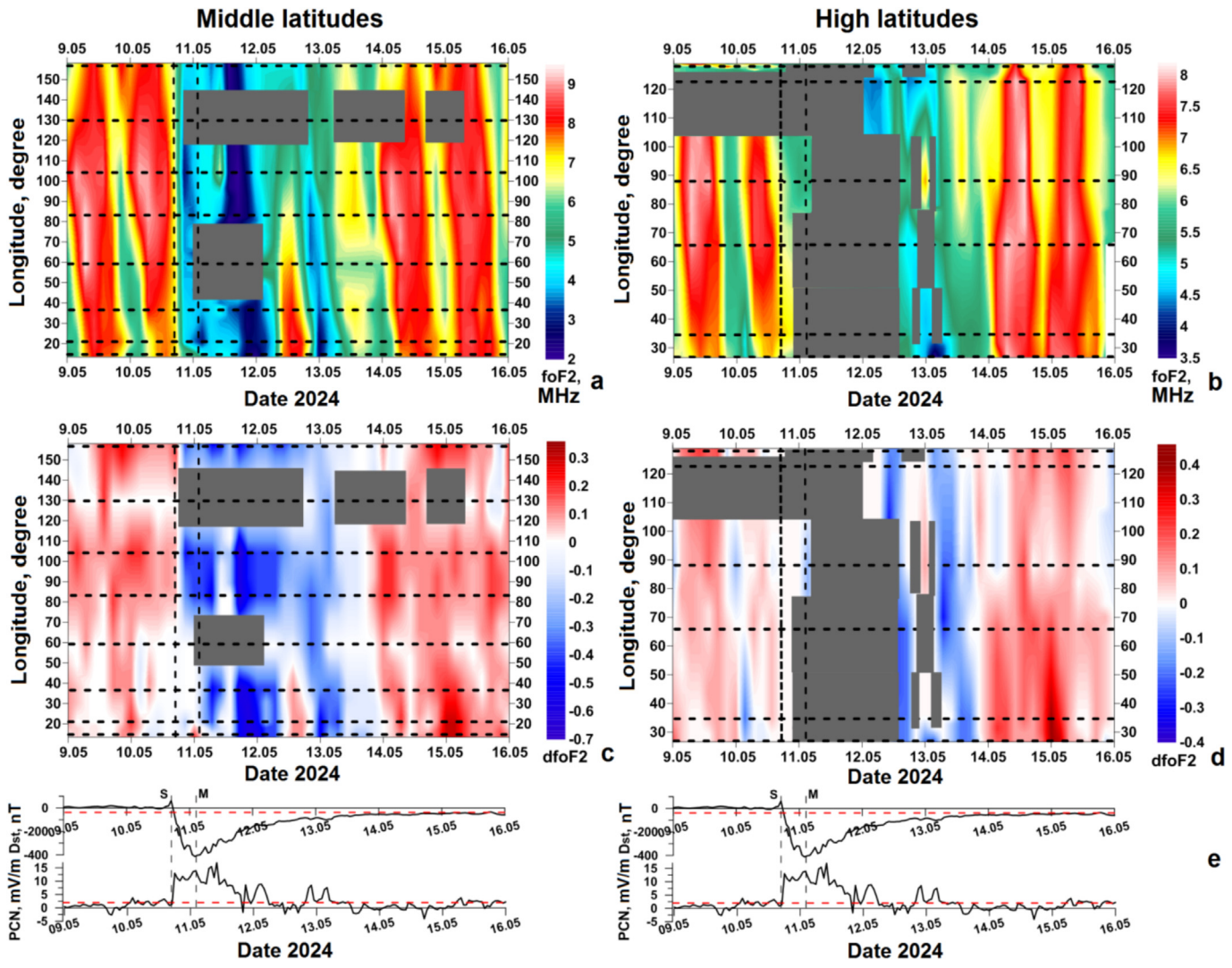

Fig. 4. Longitude-temporal variations in foF2 and dfoF2 according to data from Eurasian chains of mid- (a, c, respectively) and high-latitude (b, d) ionosondes (UT). Variations in Dst and PCN indices of geomagnetic activity (e).

threshold levels, starting from which the geomagnetic disturbance conditions at Dst ≤ −30 nT and PCN ≥ 2 mV/m are referred to storm conditions. The second vertical dashed line (right) denotes the time when the maximum storm intensity was reached, it is labeled M on the graph of Dst variations (Fig. 4e).

When comparing foF2 (and NmF2, respectively) over Eurasian mid- (4a, c) and high- (4b, d) latitudes, the first noticeable differences are those in total levels of foF2 and the amplitude of diurnal variations under quiet conditions (prior to the storm onset). This is due to the difference in seasonal illumination conditions in high- and mid-latitudes in the Northern Hemisphere. The high-latitude ionosondes in Sodankylä, Salekhard, and Zhigansk are situated along the latitude of the Arctic Circle (66.6° N), where regions beyond this latitude experience either polar day or polar night, whose durations increase progressively towards higher latitudes. At the latitudes of Norilsk (69° N), Sodankylä, Salekhard, and Zhigansk that are situated on the Arctic Circle, the polar day has not yet begun. In terms of illumination conditions, for the considered period of 9–15 May 2024, they are closer to the summer season than to the equinox. At ionospheric heights, the Sun practically does not set during the summer, which weakens the contrast between regular day-to-night variations in ionospheric parameters. Diurnal variations in foF2 are far less pronounced than under the equinox conditions. For mid-latitudes, foF2 varied from 6 to 7 to 9 MHz (Fig. 4a), for high-latitudes – from 6 to 8 MHz (Fig. 4b).

With increasing magnetic disturbance (under the conditions of ionospheric storm development), the foF2 variability in the high-latitude ionosphere is also less than in mid-latitudes, even in the case of such extremely intensive magnetic storm. Similar ionospheric effects at different latitudes were mentioned in (Araujo-Pradere et al., 2005).

Almost immediately after the superstorm onset on the evening of 10 May 2024 at 17:00 UT, all ionosondes detected a sharp drop in electron concentration NmF2 (respectively, foF2) at the height of the F2-layer maximum regardless of local time at each measurement site. This drop continued throughout the storm main phase (Fig. 4a–d). By the time the peak intensity was reached at 02:00 UT on 11 May 2024.

(Dst = −412 nT, vertical dashed line labeled M in Fig. 4e), foF2 decreased to 2–3 MHz according to mid-latitude ionosondes in Paratunka, Irkutsk, Novosibirsk, Moscow, Kaliningrad, and Juliusruh (Fig. 3c); dfo*F2* reached −0.5 to −0.7 (Fig. 4c). With the storm onset, the DPS-4 ionosonde in Yakutsk exhibited highly unstable operation (Figs. 4a,c). The ionosonde in Ekaterinburg showed a total absence of data, also known as a blackout, when the magnetic storm reached its maximum intensity. Then, technical issues arose in the operation of the Parus 3.0 ionosonde in Ekaterinburg (from 14:00 UT on 11 May until 2:30 UT on 12 May 2024) (Figs. 4a, c).

Ionograms from nearly all high-latitude ionosondes (except the DPS-4 ionosonde in Norilsk) showed complete blackouts of radio signals throughout the main phase of the magnetic storm. Shortly after the storm reached its maximum intensity, the Norilsk ionosonde also experienced a blackout. Recall that the DPS-4 ionosonde in Zhigansk was not operational for technical reasons until 12 May 2024.

Additional bursts of geomagnetic activity detected in PCN, AE, Ap, and Kp variations (Figs. 2 and 4e) during the storm recovery phase were also followed by significant decreases in electron concentration at midlatitudes according to ionosonde measurements at all longitudes of the Eastern Hemisphere – above Paratunka, Irkutsk, Novosibirsk, Moscow, Kaliningrad, and Juliusruh, except Yakutsk and Ekaterinburg, where there were technical issues in ionosonde operation. This was a negative ionospheric disturbance of a longer duration – from noon on 11 May to approximately 06:00 UT on 12 May. It was registered that foF2 dropped to 2–3 MHz (Fig. 4a), and dfoF2 dropped from −0.5 to −0.7 (Fig. 4c), i.e. down to the values observed during the main phase of the 10–11 May 2024 superstorm.

This was followed by a temporary recovery of electron concentration over midlatitudes of Eastern and Western Europe, as measured by ionosondes in Ekaterinburg (foF2 up to ~7 MHz), Moscow, Kaliningrad, and Juliusruh (foF2 up to ~8 MHz). The recovery took place during the local daytime (Fig. 4a) and reached levels of undisturbed conditions on 9–10 May 2024. However, the regions of Eastern Siberia and the Far East of Eurasia, experiencing evening and nighttime conditions, continued to remain in the phase of negative ionospheric storm: foF2 of ~4–5 MHz (Fig. 4a) and foF2 varied from −0.3 to −0.5 (Fig. 4c).

Another burst of geomagnetic disturbance was detected during the transition from 12 to 13 May 2024 (PCN, AE, Ap, and Kp indices in Figs. 2 and 4e). During this period, Dst had already increased to.

−98 nT at 22:00 UT on 12 May. This intensification of geomagnetic disturbance associated with another coronal mass ejection (CME) arriving at Earth from a sequence of solar flares on 9–11 May 2024, led to another sharp drop in electron concentration, which recovered in daytime hours on 12 May 2024. At the beginning of May 13, 2024, as recorded by ionosondes in Juliusruh, Kaliningrad, Moscow, and Ekaterinburg, foF2 decreased to ~2–3 MHz (Fig. 4a) for several hours, covering longitudes of Europe and Western Siberia (Novosibirsk ionosonde data). In the longitudinal sector of mid-latitude Eastern Siberia and the Far East, the effect of negative ionospheric storm was observed throughout the storm main phase early on 11 May 2024 and then, for the rest of the day on 11 May, 12 May and the first half of 13 May, i.e. for two and a half days (Figs. 4a, c). At different longitudes, dfoF2 varied from −0.2 to −0.5 (Fig. 4c).

From the second half of 13 May ionosphere electron concentration began to gradually return to its normal pre-storm state and increased (foF2 ~7 MHz) at all longitudes of mid-latitude Eurasia. At the end of the magnetic storm recovery phase on 14–15 May 2024, one could note a period of some increased electron concentration in the mid-latitude ionosphere over Eurasia (Figs. 4a, c). Such an increase of electron concentration can be attributed to the ionospheric aftereffect (Klimenko et al., 2018; Ratovsky et al., 2018).

When discussing the negative response of the mid-latitude ionosphere during geomagnetic disturbances, it is important to account for the well-known expansion and southward displacement of ionospheric ionization troughs from the high-latitude ionosphere. During geomagnetic storms, the auroral ionosphere shifts significantly toward the mid-latitude ionosphere. The boundaries of MIT and of other ionospheric ionization troughs (ring, high-latitude, etc.), along with the zones of particle precipitation, move toward the equator into mid-latitude regions. This leads to an increase in electron concentration gradients at these boundaries, and formation of sporadic layers of the ionosphere. During these periods, mid-latitude ionosondes record subauroral-type ionograms (Mamrukov et al., 2000). It is obvious that during the analyzed magnetic storm, MIT moved far southward beyond the latitudes of Eurasian mid-latitude ionosondes (geomagnetic latitudes 42° < GMlat < 54° N) (Yasyukevich et al., 2025; Danilchuk et al., 2025; Ponomarchuk et al., 2025). This is evidenced by numerous visual observations of auroras in areas at substantially lower latitudes (Grandin et al., 2024; Hayakawa et al., 2024).

Since the beginning of the storm's main phase (late 10 May and early 11 May 2024) until the evening of 12 May 2024, the ionosondes of the high-latitude chain in Norilsk, Salekhard, Lovozero, and Sodankylä showed a complete lack of data (radio blackout), i.e. more than one and a half days. According to Tiksi ionosonde data, the duration of

the radio signal blackout period was a little shorter, lasting until the morning of 12 May 2024. The ionosonde in Zhigansk that started working again at the beginning of 12 May 2024 showed very low foF2 ~3.5–4 MHz compared to quiet days before the storm. Such a long-lasting radio blackout included the periods of additional bursts of geomagnetic activity in PCN, AE, Ap, and Kp variations (Figs. 2 and 4e) from pre-midday hours on 11 May up to ~06:00 UT on 12 May 2024. Blackouts of radio signals, as indicated by ionosonde data, may result from a severe drop in electron concentration within F-region of the ionosphere, and also, from abnormally enhanced absorption of radiowaves in the lower ionosphere. These ionospheric effects will later be discussed with respect to their impact on the attenuation of a transmitter radio signal during vertical ionospheric sounding.

In the evening on 12 May 2024, all ionosondes of the high-latitude Eurasian chain started detecting low electron concentration (foF2 ~4–5 MHz) (Fig. 4b) when dfoF2 varied from −0.3 to −0.4 (Fig. 4d) at all longitudes. Another burst of geomagnetic disturbance that occurred during the storm recovery phase at the transition from 12 to 13 May 2024 (indices PCN, AE, Ap, and Kp in Figs. 2 and 4e) let to another radio signal blackout, clearly detected by ionosondes in Tiksi, Norilsk, Salekhard, and Lovozero (Fig. 4b), with the exception of Zhigansk and Sodankylä ionosondes. The Sodankylä ionosonde showed a very low electron concentration (foF2 ~3.5–4 MHz) and dfoF2 of approximately −0.4 over the Western Europe (Fig. 4b), while the Norilsk ionosonde detected increased electron concentration (foF2 ~6.5–7 MHz) (Figs. 4b, d) at the longitude of high-latitude Eastern Siberia. Recall that in this time interval, electron concentration in the longitude sector of mid-latitude Western Siberia, Eastern and Western Europe (Fig. 4a) was also lower than at the longitudes of Eastern Siberia and the Far East. In general, the effect of negative ionospheric storm was seen over the high-latitude region of Eurasia (similar to the mid-latitude region) throughout the main phase of the storm in the beginning of 11 May 2024 and then for the rest of 11 May, on 12 May and during the first half of 13 May, i.e. for two and a half days (Figs. 4b, d). At different longitudes, dfoF2 varied from −0.1 to −0.4 (Fig. 4d).

From the second half of 13 May, the electron concentration began recovering (gradually returning to its normal pre-storm state) in the high-latitude regions of Eastern Siberia and the Far East of Eurasia (foF2 up to ~6–6.5 MHz). Over the longitudinal sector covering Western Siberia, Eastern Europe, and Western Europe (Fig. 4b), electron concentration was lower (foF2 ~5–6 MHz). This discrepancy is most probably attributable to differences in local solar time, since dawn arrived earlier in the eastern than in the western longitude sector.

At the final stage of the recovery phase of the magnetic storm with the onset of May 14–15, 2024, electron concentration returned to near-pre-storm levels (foF2 ~6.5–7.5 MHz) at all longitudes in the high-latitude region of Eurasia (Figs. 4b, d). There was a period of increased electron concentration in the high-latitude ionosphere (Figs. 4b, d), when at night there was no decrease in the electron concentration to values in undisturbed conditions before the onset of the superstorm. The foF2 diurnal variation range was only ~1 MHz (from 6.5 to 7.5 MHz), while before SSC, the foF2 daily variation was ~2.5 MHz (from 5 to 7.5 MHz) (Fig. 4b). Thus, the ionospheric aftereffect exhibited distinct prominence across all longitudes of Eurasia at high (Figs. 4b, d) and middle latitudes (Figs. 4a, c) (Klimenko et al., 2018; Ratovsky et al., 2018). This phenomenon is unusual and interesting for high-latitudes. Moreover, the rise in electron concentration was markedly stronger over the high-latitude region than over mid-latitudes. This raises the question about the mechanism of this phenomenon.

Numerical calculations using the Global Self-Consistent Model of the Thermosphere, Ionosphere, and Protonosphere (GSC-TIP) (Namgaladze et al., 1988; Klimenko et al., 2018), and statistical analysis of data from the mid-latitude ionosondes Irkutsk and Kaliningrad (Ratovsky et al., 2018), showed that the electron concentration positive disturbances during daytime few days after the start of storm recovery phase can be induced by elevated density of atomic oxygen due to its transfer from equatorial to middle latitudes in the late recovery phase (Klimenko et al., 2018). In turn, this transfer is caused by an additional neutral gas pressure gradient from low to high latitudes. This gradient results from excessive neutral gas density at low latitudes during the main phase of a geomagnetic storm. This density is caused by oxygen transfer from auroral latitudes toward the equator. The ionization values can exceed those of quiet days prior to the onset of a magnetic disturbance. The authors compare the $[O]/[N_2]$ disturbance, as well as the electron concentration disturbance, to the pendulum oscillations, which passes from the negative phase to the positive one within a few days after the beginning of the storm recovery phase.

Thus, as the authors suggest in (Klimenko et al., 2018; Ratovsky et al., 2018), the ionospheric aftereffect of a magnetic storm should cause an earlier and more pronounced increase in electron concentration at mid- than at high-latitudes. Analysis of spatio-temporal variations in foF2 derived from high- and mid-latitude Eurasian ionosonde data (Fig. 4a–d) reveals that on 14 May 2024, the rise in electron concentration began nearly simultaneously in both mid- (Figs. 4a, c) and high-latitude (Figs. 3b, d) regions. Furthermore, during the night of 14–15 May 2024, at high-latitudes over the European region, dfoF2 relative variations were even greater (~0.4, see Fig. 4d) than at mid-latitudes (~0.3, see Fig. 4c) as compared to quiet days on 9–10 May 2024 before the magnetic storm commenced. It is probable that variations in thermodynamic parameters and the composition of thermospheric gas directly over the high-latitude zone of Eurasia during the storm recovery phase played a role.

It is necessary to take into account that the total lack of radio signal reflections (blackout) in ionograms recorded by high-latitude ionosondes during both the main and recovery phases of a magnetic storm arises from the combined action of two key factors. Firstly, there is a substantial reduction in electron concentration in the upper ionosphere, (negative ionospheric storms, which dominate the ionospheric response to enhanced geomagnetic activity). Secondly, an anomalous increase in radiowave absorption occurs in the lower ionosphere. It is known that radiowave absorption in the ionosphere is proportional to electron concentration and the frequency of collisions between electrons and neutral particles. During geomagnetic disturbances, these two parameters can be very high within the lower ionosphere (regions D and E) due to intensive ionization and plasma heating, and because energetic particles from the magnetosphere penetrate the high-latitude ionosphere along the magnetic field lines. Propagation of radiowaves to the height of F2-layer peak ionization may also be hindered by irregular thin layers of elevated electron concentration. These layers typically have thickness on the order of several kilometers and occur in the E-region (heights of 90–140 km) – sporadic Es-layers. These layers appear quite often in high and middle latitudes, especially during magnetic disturbances. As a consequence, medium and high-frequency radiowaves employed in vertical sounding are entirely absorbed within the lower layers of the ionosphere. Therefore, for a more detailed analysis of ionospheric effects caused by magnetic storms, it would be essential to additionally analyze variations in the parameter fmin, characterizing radiowave absorption in the D-region of the lower ionosphere, and foEs, describing the formation of sporadic Es-shielding layers in the E-region. However, this analysis is not within the scope of this study and will be presented in the paper (Chernigovskaya et al., 2025).

5. Results of analysis of experimental data on latitudinal and longitudinal variations in high- and mid-latitude ionospheric parameters over Eurasia during specific days of the May 2024 superstorm

Based on the measurements of the critical frequency foF2 of two Eurasian chains of ionosondes located in the high-latitude region (67°–71° N, 26°–129° E; red markers in Fig. 1a; Table 1) and in the mid-latitude region (52°–62° N, 13°–158° E); white markers in Fig. 1a; Table 2), the differences between the value of the critical frequency foF2(t, d) at the current hour t of the current day d during the storm period (i.e. from May 10, 2024) and the value foF2 at the same current hour t of the quiet day d_{quiet} before the storm onset (i.e. May 9, 2024) are calculated:

$$\Delta foF2(t,\ d) = foF2(t,\ d) - foF2(t,\ d_{quiet})$$

Fig. 5 shows maps of the longitude-latitude variations in ΔfoF2(t, d) at certain moments of time from 01:00 UT to 23:00 UT hours every 2 h during 10–12 May 2024. The black dots indicate the locations of ionosondes. Gray circular segments indicate the boundary of the day-night transition over the Eurasian territory. Vertical red lines in the Dst-variation graphs beneath each map show the current Dst at a particular moment (UT). The time interval 10–12 May 2024 covers the geomagnetically quiet period preceding the magnetic storm, the storm main phase (marked by a red arrow; SSC and the moment when Dst reaches its minimum are highlighted by red rectangles), and the early recovery phase until the end of 12 May 2024. When plotting spatial maps, missing data in the time series of ionosonde measurements were supplemented using linear interpolation based on neighboring available data points. In the same manner, foF2 data were linearly interpolated in latitude and longitude between geographical points of the considered ionosonde chains in Eurasia. In view of low spatial resolution of radiophysical measurement points and periods of radio blackouts (Figs. 4a, b), the patterns of variations in foF2 (and thus, in electron concentration at the height of maximum ionospheric ionization) during the storm main phase on 11 May and the early recovery phase on 11–12 May 2024, should be considered approximate, particularly for the high-latitude region of Eurasia.

During the main phase of the storm from 17:00 UT on 10 May to 02:00 UT on 11 May 2024 (maps are marked with red rectangles), when Dst decreased to −412 nT, episodic measurements were made only at Norilsk ionosonde. Other high-latitude ionosondes – Tiksi, Salekhard, Lovozero, and Sodankylä showed radio signal blackouts; the ionosonde in Zhigansk was nonoperational due to technical faults. Data were also missing during the early recovery phase of the magnetic storm until the end of 11 May 2024. From 12 May, the ionosonde in Zhigansk resumed its operation, and around noon on 12 May, all high-latitude chain ionosondes recommenced reporting foF2 measurement data. There were no measurement data from mid-latitude ionosondes in Yakutsk (11–12 May 2024) and Ekaterinburg (end of 10 May and all day on 11 May 2024). However, even considering the intervals of lacking ionosonde data, the dynamics of such approximate maps can be helpful in analyzing large-scale spatial ionospheric effects developing during a magnetic storm event.

The white fill on the maps means that based on ionosonde measurements, there were no changes in foF2 compared to the current UT hour under quiet geomagnetic conditions on May 9, 2024. The blue fill means that foF2 has decreased compared to the current UT hour on the quiet day of 9 May 2024. And the red fill shows a positive variability of the foF2 compared to the quiet conditions. Thus, it is possible to observe the current trend in the electron concentration response of the ionosphere when a geomagnetic disturbance develops.

Under quiet geomagnetic conditions on 10 May 2024, prior to the geomagnetic storm onset at 17:00 UT, longitude-latitude variation maps for different timepoints UT demonstrate diurnal variations in electron concentration linked to transitions between day and night conditions

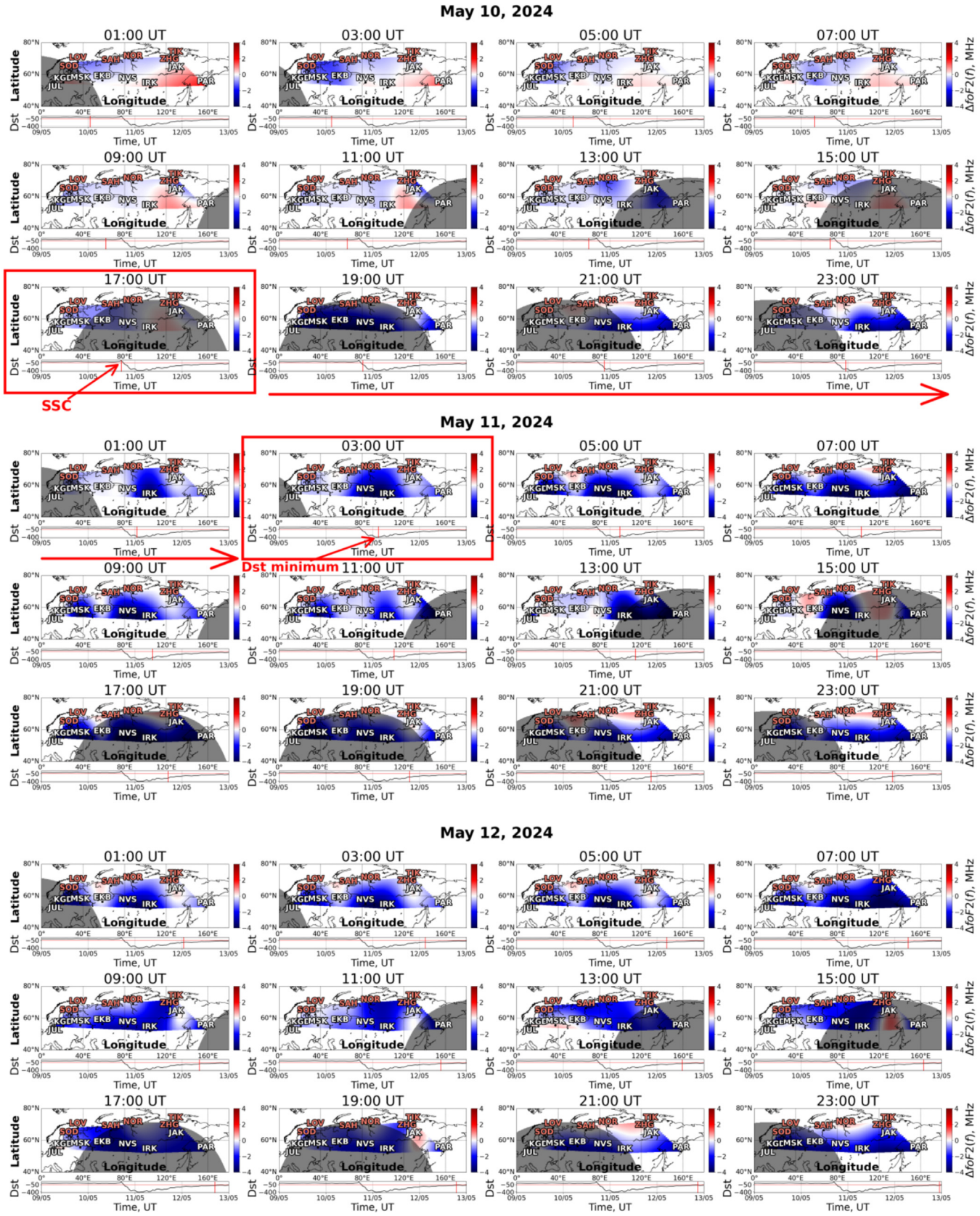

Fig. 5. Maps of longitude-latitude variations in ΔfoF2(t, d) as measured by Eurasian ionosondes at high- and mid-latitudes at timepoints from 01:00 UT to 23:00 UT every 2 h during 10–12 May 2024. Abbreviated names of ionosondes are given in Tables 1, 2. Gray circular segments indicate the boundary of the day-night transition over the Eurasian territory. Vertical red lines in the Dst-variation graphs beneath each map show the current Dst at a particular moment (UT).

(movement of the gray area bounded by the solar terminator) over different geographic regions of Eurasia. These maps show areas of negative variations (with a decrease in foF2 compared to the quiet conditions) in blue. Such areas are mostly localized over the Eurasian regions located in the night near-midnight sector. In summer, electron concentration NmF2 (and foF2, respectively) increases very rapidly after local near-midnight minimum to a daily maximum (red color on maps corresponding to 01:00, 03:00 and 15:00 UT on 10 May 2024 over the Far East, Eastern Siberia, and Europe). Following this, NmF2 exhibits slight variations during daylight hours or remains nearly constant throughout the day (white or blue color on the maps corresponding to 05:00 and 07:00 UT on 10 May 2024 across different longitudinal parts of Eurasia). Then, the evening summer maximum of electron concentration emerges, which is particularly prominent at midlatitudes (red color on the maps corresponding to 09:00 and 11:00 UT on 10 May 2024 over the Far East and Eastern Siberia regions).

During the storm's main phase immediately after the SSC event, the pattern of hourly variations in foF2 changes dramatically. Fig. 5 shows maps of longitude-latitude variations in ΔfoF2(t, d) at the moment of SSC and when Dst minimum is reached – they are highlighted by red rectangles, while maps at intermediate times during the storm's main phase are indicated by a red arrow. The patterns of periodic diurnal changes in foF2, descriptive of the summer season and the analyzed latitudinal zones, cannot be traced at all during 11–12 May 2024. Regardless of the time of day, prevailing are negative effects (blue color on maps) in electron concentration variations (ΔfoF2 to −4 MHz). Positive changes in foF2 or the constancy of the critical frequency during the current hour t are indicated by red or white color filling only over some very small spatial regions of Eurasia on longitude-latitude maps shown in Fig. 5.

It is important to account for the ionospheric effects related to additional bursts of geomagnetic disturbance that were detected in PCN, AE, Ap, and Kp variations in the early recovery phase of the storm – at 09:00–10:00 UT on 11 May, during the transitions from 11 to 12 May and from 12 to 13 May (Fig. 2), that were observed from ionosonde measurements (Fig. 4a–d).

During such enhancements of geomagnetic activity, essential decreases in electron concentration were registered. It is possible to reliably speak about a vivid manifestation of the negative ionospheric storm effect in the mid-latitude region in the Eastern Hemisphere, based on ionosonde measurements at all longitudes – above Paratunka, Irkutsk, Novosibirsk, Moscow, Kaliningrad and Juliusruh, except Yakutsk and Ekaterinburg, where ionosondes had technical issues. As repeatedly noted above, high-latitude ionosondes in Tiksi, Salekhard, Lovozero, and Sodankylä exhibited total radio signal blackouts; ionosonde in Zhigansk was nonoperational due to technical faults. Episodic measurements were made only at Norilsk ionosonde. This was a longer-lasting negative ionospheric disturbance – from noon on 11 May to approximately 06:00 UT on 12 May. In comparison to NmF2 decrease during the main phase of the magnetic storm, it had a longer duration and a comparable magnitude of the drop in electron concentration. Afterward, during the afternoon hours of 12 May 2024, there was a temporary recovery of electron concentration over midlatitudes of Eastern and Western Europe as measured by ionosondes in Ekaterinburg (foF2 up to ~7 MHz), Moscow, Kaliningrad, and Juliusruh (foF2 up to ~8 MHz). The recovery took place during the local daytime (Fig. 4a) and reached the levels of undisturbed conditions on 9–10 May 2024. But the mid-latitude regions of Eastern Siberia and the Far East of Eurasia, that were under evening and nighttime conditions, still remained in the phase of negative ionospheric storm: foF2 of ~4–5 MHz (Fig. 4a) and dfoF2 varied from −0.3 to −0.5 (Fig. 4c).

Also, a very interesting fact is that longitudinal regions with strong negative variations (as shown in maps of longitude-latitude variations in ΔfoF2(t), Fig. 5) of the F2-layer critical frequency coincide with longitude sectors of enhanced variations in GMF components during the magnetic storm (Fig. 3). Two zones with the maximum variations in GMF horizontal H-component in sectors ~40°–50° E and ~130°–135° E were identified over the mid-latitude region of Eurasia during the main (10 May 2024) and early recovery (11 May 2024) phases of the storm (Fig. 3a). We interpret these longitudinal sectors as the regions where disturbances from the high-latitude ionosphere maximally penetrated into midlatitudes. It is presumed that at these longitudes, the equatorward displacement of the boundaries of MIT and other ionization troughs (ring, high-latitude, etc.), together with the zone of active particle precipitation into mid-latitude regions was more effective. Under daylight conditions on 11–12 May 2024, longitudinal sectors of strong negative variations in ΔfoF2 compared to the quiet conditions (colored dark blue) were located over the Eastern Siberia and Eastern Europe. Regions of slightly changing foF2 values (colored white) were located between them over Western Siberia, as well as over territories of the Far East and Western Europe (Fig. 5).

6. Results of analyzing GUVI TIMED satellite data on spatio-temporal variations in atmospheric gas column [O]/[N_2] at thermospheric heights

Fig. 6 shows the maps of longitude-temporal variations in the critical frequency relative deviations (dfoF2) according to data from the mid-latitude chain of Eurasian ionosondes (Figs. 6a and 4c) and atmospheric gas column [O]/[N_2] at thermospheric (ionospheric) heights above ~100 km for mid-latitude Eurasia (54°–56° N) (Fig. 6b) from GUVI TIMED satellite measurements with UV-spectrometer (Christensen et al., 2003). Unfortunately, satellite data on [O]/[N_2] for high-latitude Eurasia (60°–65° N) are not available, presumably due to technical issues

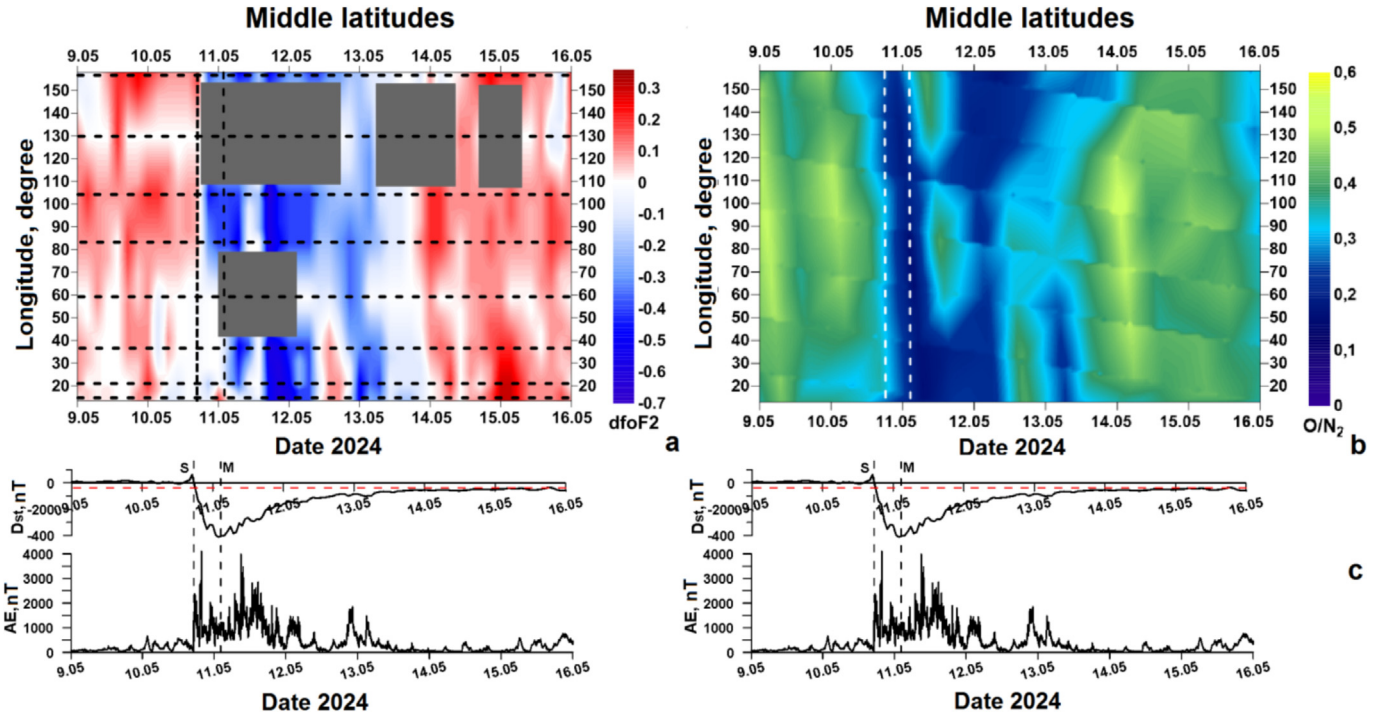

Fig. 6. Longitude-temporal variations in dfoF2 from data by mid-latitude chain of Eurasian ionosondes (a) and [O]/[N_2] (from data by GUVI TIMED measurements for the mid-latitude region (b) in May 2024 (UT). Dst and AE variations (c).

with measurements. Physical parameter [O]/[N_2] is a good indicator of negative phases of ionospheric storms (Prölss and Werner, 2002; Laštovička, 2002; Danilov, 2003; Liou et al., 2005). A reduction of the thermospheric gas [O]/[N_2] results in a decreased electron concentration within this region, leading consequently to the development of a negative ionospheric storm effect.

A strong decrease in [O]/[N_2] at thermosphere heights over all longitudes of the mid-latitude region of Eurasia (Fig. 6b) almost immediately with the onset of the geomagnetic disturbance was a consequence of complex and intense electrodynamic processes occurring under superstorm conditions in polar latitudes (variations in the AE index in Fig. 6c). A visual comparison of dfoF2 variations (Fig. 6a) with variations in the neutral composition at the same latitudes and longitudes (Fig. 6b) based on satellite measurements allows us to conclude that these parameters show a very high level of positive correlation.The longitude-temporal distribution of the [O]/[N_2] ratio explains in detail the features of the ionospheric plasma response to extreme geomagnetic disturbance that were described above. In particular, the sharp and strong decrease in foF2 in the ionosphere over mid-latitude Eurasia, amounted to reductions of 50–70 % compared to quiet-time data, which was observed almost from the moment of the SSC magnetic superstorm. This negative ionospheric storm persisted throughout the main phase and extended beyond two full days, until the evening of 13 May 2024 in the recovery phase of the magnetic storm. During the observed negative ionospheric storm, [O]/[N_2] was also very low ~0.1–0.2, it increased up to 0.3–0.4 during certain short periods for almost three days from the evening of 10 May to the evening of 13 May 2024.

A significant decrease in the electron concentration in the middle latitudes (Fig. 6a) during periods of additional bursts of geomagnetic activity in the recovery phase of the storm (variations in the PCN, AE, Ap, Kp indices in Figs. 2 and 6c) was also accompanied by corresponding periods of very low values of the [O]/[N_2] ratio (Fig. 6b). It was a lasting negative ionospheric disturbance, from noon on 11 May to approximately 06:00 UT on 12 May. A drop in the critical frequency foF2 to 2–3 MHz (Fig. 4a) and relative deviations dfoF2 varied from −0.5 to −0.7 (Figs. 4b and 6a) was recorded over Paratunka, Irkutsk, Novosibirsk, Moscow, Kaliningrad and Juliusruh, except Yakutsk and Ekaterinburg, where ionosondes had technical issues. Electron concentration decreased to the values observed during the main phase of the superstorm on 10–11 May 2024.

After that, in daylight hours on 12 May 2024, there was a temporary increase in electron concentration over the mid-latitude regions of Western (Juliusruh and Kaliningrad ionosondes) and Eastern Europe (Moscow and Ekaterinburg ionosondes) – foF2 up to ~8 MHz (Fig. 4a) and dfoF2 up to 0.1–0.3 (Figs. 4b and 6a), reaching the levels of undisturbed conditions on 9–10 May 2024. This was a local increase in electron concentration within a limited longitude sector is clearly associated with the growth

of [O]/[N_2] in the same latitude-longitude region (Fig. 6b). Apparently, the changes in the neutral thermosphere composition above 100 km could be related to a decreased intensity of electrodynamic processes, namely, currents flowing along the boundary of the auroral oval in the ionosphere (eastern and western polar electrojets), the variability of which is indicated by AE variations (Fig. 6c). However, the regions of Eastern Siberia and the Far East of Eurasia, experiencing evening and nighttime conditions, continued to remain in the phase of negative ionospheric storm: foF2 of ~4–5 MHz (Fig. 4a) and dfoF2 varied from −0.3 to −0.5 (Figs. 4c and 6a).

Another burst of geomagnetic disturbance was recorded during the transition from 12 May to 13 May 2024. (PCN, AE, Ap, and Kp indices in Figs. 2 and 6c). During this period, Dst had already increased to −98 nT at 22:00 UT on 12 May. This enhancement of geomagnetic disturbance related to the arrival of another coronal mass ejection (CME) to Earth due to a sequence of solar flares on 9–11 May 2024, again caused a drop in electron concentration over the European territory, which recovered during daylight hours on 12 May 2024 (Fig. 6a). For about half a day before noon on 13 May 2024, over the longitudes of Europe (ionosonde data from Juliusruh, Kaliningrad, Moscow and Ekaterinburg) and Western Siberia (Novosibirsk ionosonde data), foF2 decreased to ~2–3 MHz (Fig. 4a), and dfoF2 decreased from −0.4 to −0.6 (Figs. 4c and 6a). This decrease in electron concentration in the F2-region was induced by yet another wave of low [O]/[N_2] (Fig. 6b) across all longitudes of the mid-latitude region of Eurasia. Record low [O]/[N_2] values were observed over the longitudes of mid-latitude Western and Eastern Europe, and the Far East region.

In the longitudinal sector of mid-latitude Eastern Siberia and the Far East, the effect of negative ionospheric storm was observed throughout the storm main phase early on 11 May 2024 and then, for the rest of the day on 11 May, 12 May and the first half of 13 May, i.e. for two and a half days (Figs. 4a, c). At different longitudes, dfoF2 varied from −0.2 to −0.5 (Figs. 4b and 6a). Such a lasting negative disturbance of electron concentration, covering a vast Asian territory, was caused by an extreme, catastrophic drop in [O]/[N_2] according to GUVI TIMED satellite measurements during the superstorm for almost three days (Fig. 6b).

Then, from the second half of 13 May 2024, in all longitudinal sectors of the mid-latitude Eurasia, electron concentration began to increase to the pre-storm level: dfoF2 ~0–0.3 (Figs. 4b and 6a). The increase in electron concentration was associated with an increase in [O]/[N_2] over the entire mid-latitude Eurasian region (Fig. 6b).

Fig. 7 shows a sequence of maps of [O]/[N_2] global spatial distributions at thermospheric heights above ~100 km according to GUVI TIMED satellite measurements for each day from 9 May to 17 May 2024 in the Northern Hemisphere (https://guvitimed.jhuapl.edu/guvi-gallery-l3on2). The day-to-day evolution of these global maps makes it possible to visualize the dynamics and transformation of large-scale regions with low [O]/[N_2] over all longitudes and latitudes of the Northern Hemisphere.

Maps in Fig. 7 demonstrate that from the superstorm onset on the evening of 10 May (UT) 2024, during the

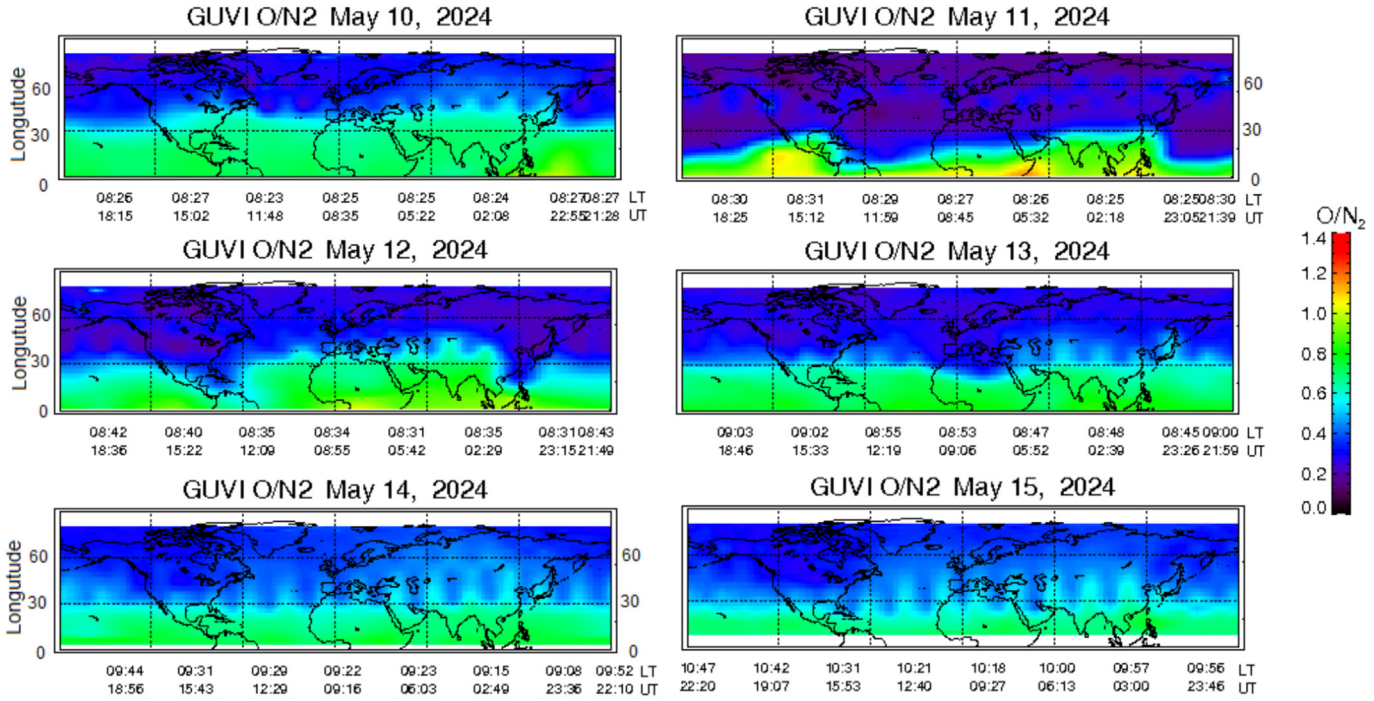

Fig. 7. Global spatial distributions of the [O]/[N_2] density ratio at thermospheric heights above ~100 km according to GUVI TIMED satellite measurements for each day 10–15 May 2024 in the Northern Hemisphere.

storm main phase on 10–11 May and then in the storm recovery phase until the end of 11 May, a vast territory throughout the Northern Hemisphere from high to subequatorial latitudes was covered a giant area with extremely low (~0.1–0.4) [O]/[N_2] density ratio at the thermosphere (ionosphere) heights. The areas of extreme equatorward penetration (latitudes lower than 10° N) were located over the Pacific and Atlantic Oceans. By May 12, 2024, the areas of maximum penetration of low [O]/[N_2] ratios to the equator (latitudes of ~10 degrees N) had shifted to the west, covering the territories of the Far East of Eurasia and North America. At the longitudes of Eurasia and the Atlantic Ocean in the Northern Hemisphere, the boundary of low [O]/[N_2] has risen to 30°–40° N. Over the central Pacific Ocean, the boundary of low [O]/[N_2] remained at ~25° N (i.e., above the northern tropic latitude). By 13 May 2024, the boundary of low [O]/[N_2] remained at ~30° N for nearly all longitudes. Only over the African continent, the region of low [O]/[N_2] protruded to latitudes 25°–30° N. It is appropriate to recall here that on 12–13 May 2024, bursts of geomagnetic activity were recorded, which could introduce variations in spatial distribution of the [O]/[N_2] ratios.

On 14 May 2024, one can note a gradual increase in [O]/[N_2] ratios (up to 0.5–0.7) over the Eurasian mid-latitudes. This growth of [O]/[N_2] ratio is evidenced by the increased electron concentration in the F2-region as measured by the Eurasian mid-latitude chain of ionosondes (Figs. 4a, c and 6a) during 14–15 May 2024.

Negative ionospheric storms are the dominant characteristic in the ionospheric response to enhanced geomagnetic activity and are usually associated with the equatorward shift of MIT region (Prölss, 1995; Rishbeth, 1998). Seaton (1956) was the first to suggest that the decrease in electron concentration may be due to variations in the composition of thermospheric neutral gas. Enhancement of the westward auroral electrojet in the high-latitude region induces neutral winds, which redistribute the neutral atmospheric composition over most of the high-latitude region and parts of the mid-latitude region. As a lighter gas, oxygen is transported more effectively than nitrogen. This, in turn, leads to a decrease in [O]/[N_2] in the upper atmosphere and, as a result, to electron concentration negative disturbances in the F-region (Mayr and Volland, 1972; Laštovička, 2002; Prölss and Werner, 2002; Danilov, 2003; Liou et al., 2005; Klimenko et al., 2015). It is the predominant effect of this mechanism that we see in the formation of the ionospheric response over the regions of high- and mid-latitude Eurasia in the conditions of the development of the May 2024 superstorm.

7. Discussion

Shortly after such a rare magnetic storm in May 2024, which exploded natural interest in this extraordinary geophysical event, articles were published containing the results of the first analysis of the registered geomagnetic, atmospheric and ionospheric effects.

The combined optical and radio-physical measurements in Eastern Siberia carried out using new scientific facilities as part of the National Heliogeophysical Complex of the Russian Academy of Sciences (NHC RAS), supported by data from global networks, demonstrated the maximum expansion of the auroral oval equatorward to ~20° N and ~20° S and consequently the expansion of the area of charged particle precipitation into the atmosphere (Yasyukevich et al., 2025). Ionospheric plasma parameters were measured using the Irkutsk Incoherent Scatter Radar (IISR; 53° N, 103° E) and the DPS-4 vertical sounding ionosonde (52° N, 104° E) on 10–16 May 2024. A clear manifold decrease in electron concentration in the F2 layer (250–300 km) was observed, with the height of the peak electron concentration increasing at night on 10 and 11 May, and decreasing again during daylight hours (Yasyukevich et al., 2025).

Similar effects were observed in the American sector (Themens et al., 2024). The effects in the high-latitude ionosphere during the geomagnetic storm on 10–11 May 2024 were investigated based on the analysis of TEC variations together with incoherent scatter radar data and ionosonde observations. During the initial phase of the magnetic storm, a significant uplift of plasma was observed. The height of the ionization maximum increased by 150–300 km, and reached 630 km. Severe heating and changes in the composition of the high-latitude thermosphere led to the complete absence of the F2-layer on 11 May 2024 (Themens et al., 2024).

During the magnetic storm in May 2024, the authors of (Kwak et al., 2024) detected significant disturbances in the upper atmosphere on both a global and local scale. The focus of the study was on the Far Eastern sector of Asia using data from space and ground-based observations. According to ground-based observations, significant effects of the negative ionospheric storm were observed in the East Asian sector, including the Korean Peninsula. These effects are associated with the thermospheric heating and with a decrease in the oxygen to nitrogen density ratio [O]/[N_2] in high-latitude regions. Magnetometers were used to detect severe variations in the components of the surface GMF over the East Asian longitudinal region that are associated with the response to PPEFs during the magnetic storm.

(Spogli et al., 2024) presented the results of studying ionospheric and geomagnetic effects during the May 2024 magnetic superstorm over the Mediterranean sector, special attention paid to Italy. In their research, they used a network of GNSS receivers, ionosondes, and magnetometers in the Mediterranean region, which contributed to a detailed analysis of the storm-induced variations. Observatories in Italy recorded the largest variation in GMF components reaching approximately 600 nT. The most noticeable ionospheric effect after the magnetic disturbance onset was a significant decrease in electron concentration

on 11 May, which led to a pronounced negative ionospheric storm identified both from variations in the critical frequency (foF2) of the F2-layer and from TEC. The authors attribute the registered effects to a decrease in the $[O]/[N_2]$ ratio in thermospheric gas. Another negative ionospheric storm effect was recorded on 13 May 2024.

(Bojilova et al., 2024) conducted a detailed study of the evolution of spatial inhomogeneities related to the ionospheric response to the geomagnetic storm on 10–11 May 2024. For their analysis, they used ionospheric anomalies represented by positive and negative relative deviations of global TEC data, whose variations were studied depending on magnetic latitude, local time, and the behavior of geomagnetic activity parameters during the event in question. Of particular interest was the analysis of the observed differences in the response of low, middle and high latitude ionosphere in the Northern and Southern hemispheres, accounting for known mechanisms of a geomagnetic storm impact on electron concentration. In the Northern Hemisphere, electron concentration exhibited an almost instantaneous negative response after the magnetic storm onset (under summertime conditions). This negatively responding region expanded southward to reach 30° N and gradually weakened by the end of 11 May 2024. In the Southern Hemisphere (under wintertime conditions), south of 50° S latitude, a region with predominant positive response of electron concentration emerged in the beginning of the storm, followed by a negative response after midnight on 11 May. According to the authors, the observed symmetric ionospheric response spanning from the equator to latitudes of 40° N and 40° S can be explainedby the expansion of a strong equatorial ionospheric anomaly formed during the storm main phase. An interesting outcome of this study is the identification of a specific longitudinal structure in the negative ionospheric response within mid-latitudes. This structure arises from the superposed effects of two structures: one resulting from the propagation of heated polar air propagating to low latitudes, creating a negative ionospheric anomaly; and another one originating from disturbances in the equatorial dynamo mechanism, producing a positive ionospheric anomaly. This superposition may lead to shifts in phase behavior. Such a peculiarity of the complex physics governing the ionospheric response at mid-latitudes during magnetically disturbed periods was emphasized in (Habarulema et al., 2016; Chernigovskaya et al., 2023). These papers focused on the series of magnetic storms in March 2012, characterized by changing positive and negative phases of the ionospheric storm across different longitudinal sectors within the mid-latitude zone of the Northern Hemisphere. According to the authors, these observed changes in ionospheric storm effects can be attributed to the superposition of competing processes affecting ionospheric ionization. Sources of these processes belong to both the auroral ionosphere (a series of intense solar activity events that led to geomagnetic storms on 7, 9, 12, 15 March 2012 and caused essential disturbance in the atmosphere and ionosphere in high-latitudes), and the equatorial ionosphere (the super-fountain effect in subequatorial latitudes on 7–10 March 2012).

(Ponomarchuk et al., 2025) used data from vertical and oblique soundings of the ionosphere with a continuous chirp signal to investigate the effects of an extreme magnetic storm on 10–13 May 2024 that occurred in the Asian part of Russia. They identified specific characteristics of ionospheric disturbances induced by the magnetic storm, including: prolonged negative ionospheric disturbance is characterized by significant reductions in the critical frequency of the F2-layer and the maximum observed frequencies along radio propagation paths; shielding of reflections from the ionospheric F-layer by sporadic Es-layer, and enhanced absorption of HF signals. Correlations were found between, on the one hand, variations in ionospheric parameters and the maximum observed frequencies of HF radiowave propagation modes, and, on the other hand, the spatial locations of the main ionospheric trough and the equatorial boundary of the electron diffusion precipitation zone. Following the results of modeling the invariant latitude of the MIT bottom according to the model (Deminov and Shubin, 2018), on 10–13 May 2024, the Novosibirsk and Irkutsk ionosondes were located at latitudes south of the polar wall or the MIT bottom in the evening and night sectors of local time. This is confirmed by the results of reconstructing the polar oval location using DMSP SSUSI satellite data (https://ssusi.jhuapl.edu/gal_edr-aur_cs).

A radically different response was observed in the ionosphere during the initial phase of the magnetic storm in the low latitude region.

(Tulasi et al., 2024), based on the global TEC variation analysis, noted the effect of a strong positive ionospheric storm that lasted for several hours on the dayside of the ionosphere from low to middle latitudes (±45°) due to enhanced equatorial ionization anomaly on 10 May 2024. In the American longitudinal sector, TEC increased sharply by more than 100 % compared to the previous quiet day on 9 May. The crests of the equatorial anomaly shifted significantly poleward on 10 May 2024 relative to 9 May 2024. This suggests that strong PPEFs prevailed over the equatorial latitudes, which led to the effect of the equatorial fountain enhancement and the equatorial anomaly during this period. The combined effect of enhanced equatorial fountain and enhanced equatorial neutral wind, which uplifts the F-region to the heights of reduced recombination, led to such a strong positive ionospheric storm.

(Singh et al., 2024) presented the results of analyzing the ionospheric response at the equatorial and low latitudes, which was observed in the Peruvian sector using the Jicamarca Incoherent Scatter Radar (11.9° S, 76.8° W, magnetic inclination 1° N) and associated instruments, to an extremely rare G5-level geomagnetic storm in May 2024. On the Earth's dayside, due to strong PPEFs, the vertical drift of plasma and the equatorial electric jet enhanced significantly within 2–3 h and remained unchanged between 17:00 and 19:00 UT (12:00 and 14:00 LT). At the same

time, vertical plasma drift in the crossed electric and magnetic fields ExB elevated the equatorial ionosphere, creating a super-plasma fountain on the evening side and transferring the electron concentration to higher latitudes. A huge gain in electron concentration (~1325 %, from 11 to 142 TECu) was observed from ~20° to 50° S between 20:00 and 04:00 UT (15:00–23:00 LT). During the night, the combined action of penetrating electric fields and disturbed dynamo-generated electric fields caused a significant increase (~530 km) in the virtual height of the ionosphere.

The authors of (Danilchuk et al., 2025) investigate the effect on the ionosphere and the kinematic precise positioning of GPS points during the main phase of the extreme geomagnetic storm in May 2024. Global ionospheric and ROTI maps were used to analyze the dynamics of the ionosphere. The auroral oval expanded into the low-latitude region: down to 30° N in the American sector and down to 45° N in the Europe–Asian sector during the main phase of the geomagnetic storm. The crest of the equatorial anomaly became significantly higher (up to 200 TECu) and shifted poleward in the American sector. Counter-propagation allowed the equatorial anomaly to cross the boundary of the auroral oval. Positioning errors near the auroral oval boundary increased 1.5–5 times at the boundary of the auroral oval. The authors summarized that the geomagnetic storm had a profound effect on the ionosphere and significantly reduced the positioning accuracy, posing risks to the functioning of various systems reliant on navigation and communications.

(Foster et al., 2024) combined TEC data from a spatially distributed network of GNSS (Global Navigation Satellite System) receivers. They also used data from magnetometer chains and auroral observations by civil scientists to present a detailed global picture of variations in ionospheric and thermospheric parameters that occurred at the peak of the 10–11 May 2024 extreme geomagnetic storm. Within a 20-minute interval, vertical TEC increased sharply (by ~50 TECu) at an unusually low latitude (~45°) and showed a rapid azimuthal expansion across the entire continent. The intensive red aurora observed in these regions indicates that the significant TEC enhancement was caused by extremely intense precipitation of low-energy particles into the ionosphere, which aligns with the conclusions in (Grandin et al., 2024).

(Jain et al., 2025) studied the ionospheric response near the equatorial anomaly crest during the super-intense geomagnetic storm on 10–11 May 2024. The ionospheric response was observed in Bhopal, India (23.2° N, 77.4° E) using vertical total electron content (vTEC). It was noted that the magnetic storm had both positive and negative effects on vTEC. The increase in vTEC (24–50 %) in the storm main phase can be explained by PPEFs, and the decrease in vTEC in the storm recovery phase – by changes in the composition of thermospheric gas and ionospheric disturbance dynamic electric fields (DDEFs).

Summary of only some studies devoted to the global geophysical effects of the May 2024 magnetic superstorm shows that their authors consistently report a wide variety of atmospheric and ionospheric responses. The registered features of ionospheric effects (positive or negative ionospheric storm effects, or transitions between them) depend largely on geographic location of these regions and local time effects (solar illumination conditions).

In the current study, based on ionosonde measurements, we recorded the effects of a powerful negative ionospheric storm over mid- and high-latitude regions of Eurasia during the analyzed geomagnetic storm. Our findings correspond to results reported in (Themens et al., 2024; Kwak et al., 2024; Spogli et al., 2024; Bojilova et al., 2024; Yasyukevich et al., 2025; Ponomarchuk et al., 2025), where the authors analyzed variations in ionospheric parameters in the main and recovery phases of the magnetic superstorm in mid- and high-latitude regions of the Northern Hemisphere. All these studies suggest that the immediate cause of nearly instantaneous drop in ionospheric electron concentration in the Northern Hemisphere right after the onset of a geomagnetic storm can is primarily attributed to the reduced $[O]/[N_2]$ ratio in high-latitude regions, coupled with the rapid penetration of heated high-latitude neutral gas with modified composition due to strong meridional wind from the pole towards the equator.

The development of the ionospheric response to the magnetic superstorm in May 2024 appears to have followed a typical summer scenario, characterized by a predominant negative ionospheric storm effect (Burešová et al., 2007; Ratovsky et al., 2020). This finding supports the existence of seasonal patterns in the probability of positive or negative phases of ionospheric storms. A similar positive ionospheric storm effect was noted in (Chernigovskaya et al., 2021; Chernigovskaya et al., 2024a) during an extreme magnetic storm in June 2015, as measured by the same chains of Eurasian ionosondes. In contrast to the summer scenario, measurements from the same chains of Eurasian ionosondes and GPS/GLONASS receivers during the extreme magnetic storm in March 2015 (Chernigovskaya et al., 2021; Chernigovskaya et al., 2024a, b) and a series of magnetic storms in March 2012 (Chernigovskaya et al., 2023), revealed a scenario where the ionospheric effect involved transition from a positive ionospheric storm to a negative one in the main phase of the magnetic storm.

In this regard, it is appropriate to mention the superstorms on October 29–31 (Dst = −401 nT) and November 20 (Dst = −472 nT) 2003 (Halloween storms). The ionospheric response in the Northern Hemisphere to the geomagnetic superstorms in October–November 2003 was not as uniform and global as for the storm in May 2024. Brief overview of the results of the analysis of ionospheric effects of superstorms in October–November 2003 (e.g., Blanch et al., 2005; Ermolaev et al., 2005; Kane, 2005; Uma et al., 2012) shows significant differences in the ionospheric response to the events of 2003 compared to the storm of May 2024.

The ring of active auroras expanded and shifted equatorward during the main phase of the 2003 superstorms. Over the south of Eastern Siberia mid-latitude auroras associated with increased emission in the 630 nm line were observed at the Tori station in the post-midnight sector during the main phases of superstorms (Ermolaev et al., 2005).

Kane (2005) analyzed the global ionospheric response using data from 83 ionosondes from the NGDC SPIDR data center for the October 2003 superstorm event. Electron density depressions (negative ionospheric storms) were found for high northern latitudes. For northern mid- and low-latitudes, there were very strong positive effects on October 29, 2003, during the main phase of the storm, followed by negative effects the next day. Thus, a change in the effect of a positive ionospheric storm to a negative one was observed. There were no troughs at high northern latitudes for the morning and evening hours, but there were troughs for the night. For mid- and low-latitudes, some longitudes showed strong negative effects in the early morning, as expected, but some longitudes showed strong positive effects in the midday and evening hours. Thus, there were many deviations from the model predictions. The deviations were irregular, indicating significant local ionospheric effects superimposed on the general patterns. A puzzling feature was the presence of strong positive effects within 24 h of the storm's onset. This may have been a manifestation of pre-storm enhancements of foF2.

A negative effect of the ionospheric storm was detected based on foF2 measurements by the mid- and low-latitude ionosondes WKA (45.2° N, 141.1° E), KOB (35.4° N, 139.29° E) and YAG (31.2° N, 130.37° E) (Japanese and Indian longitude sectors) during the magnetic storm of November 20, 2003. At the same time, the near-equator ionosonde WTR (17.7° N, 83.3° E) showed a positive effect of the ionospheric storm, and the even closer to the equator ionosonde TRV (8.5° N, 77° E) again showed a negative effect in the electron density at the height of the F2-layer of the ionosphere during the main phase of the geomagnetic storm of November 20, 2003 (Uma et al., 2012). The TEC GIMs also reflected these longitudinal-latitudinal features of the ionospheric response quite well. They showed that a latitudinal broadening of the equatorial ionization anomaly (only up to ~25° N) and an enhancement (by ~80–100 TECu) did occur.

(Blanch et al., 2005) discussed effects observed on the ionosphere over the mid-latitude European sector produced by the 19–23 November 2003 geomagnetic storm, using data from ground ionosonde at Chilton (51.5° N; 359.4° E), Pruhonice (50.0° N; 14.6° E) and El Arenosillo (37.1° N; 353.3° E), jointly with GPS data. It is noted that during the superstorm, two ionospheric effects were recorded: (1) the presence of well-developed anomalous storm layers Es, observed at latitudes up to 37° N, and (2) the formation of two thin separate latitudinal belts of reduced (negative effect in the range of 55-45° N) and increased (positive effect in the range of 45-30° N) electron density in the European evening sector during the main phase of the storm. It was concluded that the 28 October – 5 November 2003 geomagnetic storm was stronger (the highest solar wind speed was 1850 km/s), but the effects on the Earth's ionosphere in the mid-latitude European sector were more important during the 19–23 November 2003 geomagnetic storm.

8. Conclusions

Based on the analysis of data from mid- and high-latitude Eurasian ionosonde chains, magnetometer records from INTERMAGNET and Russian observatories along with GUVI TIMED satellite measurements of thermospheric gas column $[O]/[N_2]$ above ~100 km, this study investigates the ionospheric response to the exceptionally intense magnetic superstorm in May 2024 and draws the following conclusions.

1. Almost immediately after the initial phase of a geomagnetic superstorm a sharp drop of electron concentration was recorded at the height of the F2-layer maximum over regions of mid- and high-latitude Eurasia, regardless of the local time at each measurement site. At the stage of reaching the maximum intensity of the magnetic storm, the ionosonde in Ekaterinburg and almost all ionosondes of the high-latitude chain (Norilsk, Salekhard, Lovozero, Sodankulya) registered radio signal blackout until May 12, 2024, i.e. more than one and a half days. Thus, strong effects of a negative ionospheric storm were noted in both high- and mid-latitude regions during the main and in early recovery phase of the magnetic storm.
2. With increasing magnetic disturbance (under the conditions of ionospheric storm development), foF2 variability in the high-latitude ionosphere is less than in mid-latitudes, even in the case of such extremely intensive magnetic storm.
3. With the onset of the magnetic storm, variability of the GMF components was more pronounced in mid-latitudes and increased by an order of magnitude: from 80 to 800 nT for H-component, and from 60 to 600 nT for Z-component min certain longitudinal sectors. At high-latitudes (near ~70° N), GMF variability is more uniform in longitude, but longitudinal inhomogeneities in GMF variations are also evident.
4. A very interesting fact is that longitudinal regions with strong negative variations according to maps of ΔfoF2 (t) longitude-latitude variations coincide with longitudinal sectors of enhanced variations in GMF H-component in sectors ~40°–50° E and ~130°–135° E over the mid-latitude region of Eurasia.
5. MIT and other ionization troughs (ring, high-latitude, etc.), together with the zones of active particle precipitation (auroral oval) penetrated far southward beyond the latitudes of Eurasian mid-latitude ionosondes (geomagnetic latitudes 42°<GMlat < 54° N).

6. Additional bursts of geomagnetic activity in the storm's recovery phase in certain time intervals on 11–13 May 2024 were also followed by significant and long-lasting decreases in electron concentration in mid-latitudes and another radio signal blackout for several hours in high-latitudes, like in the main phase of the magnetic storm on 10–11 May 2024.
7. At the end of the magnetic storm recovery phase, from the second half of day on 14 May and 15 May 2024, an aftereffect of geomagnetic storm was observed over Eurasia. The increase in electron concentration began nearly simultaneously in both mid- and high-latitude regions. Moreover, at high-latitudes over the European region on the night of 14–15 May 2024, relative variations dfoF2 were even greater (~0.4) than at mid-latitudes (~0.3) as compared to quiet days on 9–10 May 2024. The fact of observing this phenomenon in the high-latitude region is unusual and very interesting.
8. A sharp and strong decrease in foF2 (~50–70 percent of foF2 values under quiet conditions) observed in the ionosphere of mid-latitude Eurasia almost from the SSC and continued throughout the main phase and for more than two days until the evening of 13 May 2024 in the recovery phase of the magnetic storm was caused by an extreme, catastrophic drop of $[O]/[N_2]$ density ratio in the thermosphere during the superstorm in May 2024 for almost three days.

Declaration of competing interest

The authors declare that they have no known competing financial interests or personal relationships that could have appeared to influence the work reported in this paper.

Acknowledgments

This work was financially supported by the Russian Science Foundation (Project No. 25-17-00187, https://rscf.ru/en/project/25-17-00187/). The work was supported by the Ministry of Science and Higher Education of the Russian Federation for conducting observations and primary data processing. The results were obtained using the equipment of Shared Equipment Center "Angara" http://ckp-rf.ru/ckp/3056/.

Observations and primary data processing partially were carried out with the support of the Ministry of Science and Higher Education of the Russian Federation (project FWZZ-2022-0019); within the framework of a state assignment (state registration number 122011700182-1); within the framework of a state assignment (state registration number. № 122011700172-2); within the framework of paragraph 6.2 of the Roshydromet research and development plan "Development of methods and means for ground-based monitoring of the geophysical situation over the Arctic."

Data from Sodankylä and Juliusruh ionosondes were taken from the UK Solar System Data Center (https://www.ukssdc.ac.uk).

The results presented in this paper rely on data collected at magnetic observatories. We thank the national institutes for support and INTERMAGNET for promoting high standards of magnetic observatory practice (https://www.intermagnet.org).

The GUVI TIMED data used in this work is provided with the support of the NASA MO&DA program. The GUVI instrument was devised and built by the Aerospace Corporation and the Johns Hopkins University. The scientific supervisor is Larry J. Paxton.

References

Aladjev, G.A., Evstafiev, O.V., Mingalev, V.S., Mingaleva, G.I., Tereshchenko, E.D., Khudukon, B.Z., 2001. Interpretation of ionospheric F-region structures in the vicinity of ionization trough observed by satellite radio tomography. Ann. Geophys. 19, 25–36.

Araujo-Pradere, E.A., Fuller-Rowell, T.J., Codrescu, M.V., Bilitza, D., 2005. Characteristics of the ionospheric variability as a function of season, latitude, local time, and geomagnetic activity. Radio Sci. 40, RS5009. https://doi.org/10.1029/2004RS003179.

Berger, T.E., Dominique, M., Lucas, G., Pilinski, M., Ray, V., Sewell, R., Sutton, E.K., Thayer, J.P., Thiemann, E., 2023. The thermosphere is a drag: the 2022 Starlink incident and the threat of geomagnetic storms to low earth orbit space operations. Space Weather. 21 (3), 1–15. https://doi.org/10.1029/2022SW003330.

Blanch, E., Altadill, D., Boška, J., Buresova, D., Hernández-Pajares, M., 2005. November 2003 event: effects on the Earth's ionosphere observed from ground-based ionosonde and GPS data. Ann. Geophys. 23, 3027–3034, SRef-ID: 1432-0576/ag/2005-23-3027.

Bojilova, R., Mukhtarov, P., Pancheva, D., 2024. Global ionospheric response during extreme geomagnetic storm in May 2024. Remote Sens. 16, 4046. https://doi.org/10.3390/rs16214046.

Buonsanto, M.J., 1999. Ionospheric storms – a review. Space Sci. Rev. 88, 563–601.

Burešová, D., Laštovička, J., de Franceschi, G., 2007. Manifestation of Strong Geomagnetic Storms in the Ionosphere above Europe. In: Lilensten J. (ed.), Space Weather Springer, 185–202.

Burešová, D., Laštovička, J., 2007. Pre-storm enhancements of foF2 above Europe. Adv. Space Res. 39 (8), 1298–1303. https://doi.org/10.1016/j.asr.2007.03.003.

Chernigovskaya, M.A., Ratovsky, K.G., Setov, A.G., Khabituev, D.S., Kalishin, A.S., Dolgacheva, S.A., Stepanov, A.E., Belinskaya, A.Y., Bychkov, V.V., Grigorieva, S.A., Panchenko, V.A., Timchenko, A.V., 2025. Spatio-temporal variability of ionospheric parameters over Eurasia at meddle and high latitudes during the superstorm in May 2024. Geomagn, Aeron (in press).

Chernigovskaya, M.A., Ratovsky, K.G., Zherebtsov, G.A., Setov, A.G., Khabituev, D.S., Kalishin, A.S., Stepanov, A.E., Belinskaya, A.Y., By-chkov, V.V., Grigorieva, S.A., Panchenko, V.A., 2024a. Ionospheric response over the high and middle latitude regions of Eurasia according to ionosonde data during the severe magnetic storm in March 2015. Solar-Terrestrial Phys. 10 (4), 46–58. https://doi.org/10.12737/stp-104202406.

Chernigovskaya, M.A., Setov, A.G., Ratovsky, K.G., Kalishin, A.S., Stepanov, A.E., 2024b. Variability of ionospheric ionization over Eurasia according to data from a high-latitude ionosonde chain during extreme magnetic storms in 2015. Solar-Terrestrial Phys. 10 (2), 34–47. https://doi.org/10.12737/stp-102202404.

Chernigovskaya, M.A., Shpynev, B.G., Yasyukevich, A.S., Khabituev, D. S., Ratovsky, K.G., Belinskaya, A.Y., Stepanov, A.E., Bychkov, V.V., Grigorieva, S.A., Panchenko, V.A., Kouba, D., Mielich, J., 2021. Longitudinal variations of geomagnetic and ionospheric parameters in the Northern Hemisphere during magnetic storms according to multi-instrument observations. Adv. Space Res. 67 (2), 762–776. https://doi.org/10.1016/j.asr.2020.10.028.

Chernigovskaya, M.A., Yasyukevich, A.S., Khabituev, D.S., 2023. Ionospheric longitudinal variability in the Northern Hemisphere during magnetic storms in March 2012 from ionosonde and GPS/GLONASS data. Solar-Terrestrial Phys. 9 (4), 99–110. https://doi.org/10.12737/stp-94202313.

Christensen, A.B., Paxton, L.J., Avery, S., et al., 2003. Initial observations with the Global Ultraviolet Imager (GUVI) on the NASA TIMED satellite mission. J. Geophys. Res. 108 (A12), 1451. https://doi.org/10.1029/2003JA009918.

Danilchuk, E., Yasyukevich, Y., Vesnin, A., Klyusilov, A., Zhang, B., 2025. Impact of the May 2024 extreme geomagnetic storm on the ionosphere and GNSS positioning. Remote Sens. 17, 1492. https://doi.org/10.3390/rs17091492.

Danilov, A.D., 2003. Long-term trends of foF2 independent on geomagnetic activity. Ann. Geophys. 21 (5), 1167–1176.

Danilov, A.D., 2013. Response of region F to geomagnetic disturbances (review). Heliogeophys. Res. 5, 1–33 (In Russian).

Danilov, A.D., Konstantinova, A.V., 2019. Behavior of the ionospheric F region prior to geomagnetic storms. Adv. Space Res. 64, 1375–1387. https://doi.org/10.1016/j.asr.2019.07.014.

Deminov, M.G., Shubin, V.N., 2018. Empirical model of the location of the main ionospheric trough. Geomagn. Aeron. 58 (3), 348–355. https://doi.org/10.1134/S0016793218030064.

Enell, C.-F., Kozlovsky, A., Turunen, T., Ulich, T., Välitalo, S., Scotto, C., Pezzopane, M., 2016. Comparison between manual scaling and Autoscala automatic scaling applied to Sodankylä Geophysical Observatory ionograms. Geosci. Instrum. Method. Data Syst. 5, 53–64. https://doi.org/10.5194/gi-5-53-2016.

Ermolaev, YuI., Zelenyi, L.M., Zastenker, G.N., et al., 2005. Solar and heliospheric disturbances that resulted in the strongest magnetic storm of November 20, 2003. Geomagnet. Aeronomy 45 (1), 20–46.

Foster, J.C., Erickson, P.J., Nishimura, Y., Zhang, S.R., Bush, D.C., Coster, A.J., Meade, P.E., Franco-Diaz, E., 2024. Imaging the May 2024 extreme aurora with ionospheric total electron content. Geophys. Res. Lett. 51, e2024GL111981. https://doi.org/10.1029/2024GL111981.

Gopalswamy, N., Yashiro, S., Michalek, G., Xie, H., Lepping, R.P., Howard, R.A., 2005. Solar source of the largest geomagnetic storm of cycle 23. Geophys. Res. Lett. 32, 12. https://doi.org/10.1029/2004GL021639.

Grandin, M., Bruus, E., Ledvina, V.E., Partamies, N., Barthelemy, M., Martinis, C., Dayton-Oxland, R., Gallardo-Lacourt, B., Nishimura, Y., Herlingshaw, K., Thomas, N., Karvinen, E., Lach, D., Spijkers, M., Bergstrand, C., 2024. The geomagnetic superstorm of 10 May 2024: Citizen science observations. EGUsphere [preprint]. https://doi.org/10.5194/egusphere-2024-2174.

Habarulema, J.B., Katamzi, Z.T., Yizengaw, E., et al., 2016. Simultaneous storm time equatorward and poleward large-scale TIDs on a global scale. Geophys. Res. Lett. 43, 6678–6686.

Hayakawa, H., Ebihara, Y., Mishev, A., et al., 2024. The solar and geomagnetic storms in May 2024: a flash data report. Astrophys. J. https://doi.org/10.3847/1538-4357/ad9335.

Huang, C.M., 2013. Disturbance dynamo electric fields in response to geomagnetic storms occurring at different universal times. J. Geophys. Res.: Space Phys. 118, 496–501. https://doi.org/10.1029/2012JA018118.

Jain, A., Trivedi, R., Jain, S., Choudhary, R.K., 2025. Effects of the super intense geomagnetic storm on 10-11 May, 2024 on total electron content at bhopal. Adv. Space Res. 75 (3). https://doi.org/10.1016/j.asr.2024.09.029.

Kalishin, A.S., Blagoveshchenskaya, N.F., Troshichev, O.A., Frank-Kamenetskii, A.V., 2020. FGBU "AARI". Geofizicheskie issledovaniya v vysokikh shirotakh (Geophysical research in high latitudes). Vestnik RFFI. Antarktida i Arktika. Polyarnye Issledovaniya. 3–4 (107–108), 60–74. https://doi.org/10.22204/2410-4639-2020-106-107-3-4-60-78 (in Russian).

Kane, R.P., 2005. onospheric foF2 anomalies during some intense geomagnetic storms. Ann. Geophys. 23, 2487–2499. https://doi.org/10.5194/angeo-23-2487-2005.

Karpachev, A., 2021. Sub-auroral, mid-latitude, and low-latitude troughs during severe geomagnetic storms. Remote Sens. 13 (3), 534. https://doi.org/10.3390/rs13030534.

Klimenko, M.V., Klimenko, V.V., Bessarab, F.S., Zakharenkova, I.E., Kotova, D.S., Nosikov, I.A., et al., 2015. Influence of geomagnetic storms of September 26–30, 2011, on the ionosphere and radiowave propagation. I. Ionospheric effects. Geomagn. Aeron. 55 (6), 744–762. https://doi.org/10.1134/S0016793215050072.

Klimenko, M.V., Klimenko, V.V., Despirak, I.V., Zakharenkova, I.E., Kozelov, B.V., Cherniakov, S.M., Andreeva, E.S., Tereshchenko, E. D., Vesnin, A.M., Korenkova, N.A., Gomonov, A.D., Vasiliev, E.B., Ratovsky, K.G., 2018. Disturbances of the thermosphere-ionosphere-plasmasphere system and auroral electrojet at 30°E longitude during the St. Patrick's Day geomagnetic storm on 17–23 March 2015. J. Atmos. Sol. Terr. Phys. 180, 78–92. https://doi.org/10.1016/j.jastp.2017.12.017.

Krasheninnikov, I., Pezzopane, M., Scotto, C., 2010. Application of Autoscala to ionograms recorded by the AIS-Parus ionosonde. Comput. Geosc. 36, 628–635. https://doi.org/10.1016/j.cageo.2009.09.013.

Kwak, Y.S., Kim, J.H., Kim, S., et al., 2024. Observational overview of the May 2024 G5-level geomagnetic storm: from solar eruptions to terrestrial consequences. J. Astron. Space Sci. 41 (3), 171–194. https://doi.org/10.5140/JASS.2024.41.3.171.

Laštovička, J., 2002. Monitoring and forecasting of ionospheric space weather effects of geomagnetic storms. J. Atmos. Solar-Terr. Phys. 64, 697–705. https://doi.org/10.1016/S1364-6826(02)00031-7.

Liou, K., Newell, P.T., Anderson, B.J., Zanetti, L., Meng, C.-I., 2005. Neutral composition effects on ionospheric storms at middle and low latitudes. J. Geophys. Res. 110, A05309. https://doi.org/10.1029/2004JA010840.

Loewe, C.A., Prölss, G.W., 1997. Classification and mean behavior of magnetic storms. J. Geophys. Res. 102 (A7), 14209–14213.

MacDougall, J.W., Grant, I.F., Shen, X., 1995. The Canadian advanced digital ionosonde: design and results. WDC A for Solar-Terrestrial Physics, Report UAG-104, Boulder, Colorado, USA, 21–27.

Mamrukov, A.P., Khalipov, V.L., Filippov, L.D., Stepanov, A.E., Zikrach, E.H.K., Smirnov, V.F., Shestakova, L.V., 2000. Geofizicheskaya informatsiya po naklonnym radiootrazheniyam v vysokikh shirotakh i ikh klassifikatsiya (Geophysical information on oblique radio reflections at high latitudes and their classification). Issledovaniya po geomagnetizmu, aehronomii i fizike Solntsa (Research on geomagnetism, aeronomy and solar physics). Novosibirsk: Izd-Vo SB RAS 111, 14–27 (in Russian).

Matsushita, S., 1959. A study of the morphology of ionospheric storms. J. Geophys. Res. 64 (3), 305–321. https://doi.org/10.1029/JZ064i003p00305.

Mayr, H.G., Volland, H., 1972. Magnetic storm effects in the neutral composition. Planet. Space Sci. 20, 379.

Mendillo, M., 2006. Storms in the ionosphere: patterns and processes for total electron content. Rev. Geophys. 44, RG4001. https://doi.org/10.1029/2005RG000193.

Mikhailov, A.V., 2000. Ionospheric F2-layer storms. Física De La Tierra. 12, 223–262.

Namgaladze, A.A., Korenkov, Y.N., Klimenko, V.V., et al., 1988. Global model of the thermosphere-ionosphere-protonosphere system. PAGEOPH. 127 (2–3), 219–254.

Øvstedal, O., 2002. Absolute positioning with single-frequency GPS receivers. GPS Solutions. 5 (4), 33–44. https://doi.org/10.1007/PL00012910.

Podlesnyi, A.V., Brynko, I.G., Kurkin, V.I., Berezovsky, V.A., Kiselev, A. M., Petuchov, E.V., 2013. Multifunctional chirp ionosonde for

monitoring the ionosphere. Heliogeophysical Research. 4, 24–31 (in Russain).
Polyakov, V.M., Shchepkin, L.A., Kazimirovsky, E.S., Kokourov, V.D., 1968. Ionospheric processes. Nauka, Novosibirsk, p. 535 (in Russian).
Ponomarchuk, S.N., Zolotukhina, N.A., Kurkin, V.I., Belinskaya, A.Y., Grozov, V.P., Oinats, A.V., Poddelsky, A.I., Podlesnyi, A.V., Cedrik, M.V., 2025. The effects of magnetic storm on May 10–13, 2024 in the asian region on Russia from ionospheric sounding with a continuous chirp signal. Solar-Terrestrial Phys. 11 (4). https://doi.org/10.12737/szf-114202504.
Prölss, G.W., 1995. Ionospheric F-region storms. In: Volland H. (ed.), Handbook of atmospheric electrodynamics. CRC Press, Boca Raton. 2, 8, 195–248.
Prölss, G.W., Werner, S., 2002. Vibrationally excited nitrogen and oxygen and the origin of negative ionospheric storms. J. Geophys. Res. 107 (A2), 1016. https://doi.org/10.1029/2001JA900126.
Ratovsky, K.G., Klimenko, M.V., Klimenko, V.V., Chirik, N.V., Korenkova, N.A., Kotova, D.S., 2018. Aftereffects of geomagnetic storms: statistical analysis and theoretical explanation. Solar-Terrestrial Phys. 4 (4), 26–32. https://doi.org/10.12737/stp-44201804.
Ratovsky, K.G., Klimenko, M.V., Yasyukevich, Y.V., et al., 2020. Statistical analysis and interpretation of high-, mid-and low-latitude responses in regional electron content to geomagnetic storms. Atmosphere. 11 (12), 1308. https://doi.org/10.3390/atmos11121308.
Reinisch, B.W., Haines, D.M., Bibl, K., et al., 1997. Ionospheric sounding support of over-the-horizon radar. Radio Sci. 32 (4), 1681–1694.
Rishbeth, H., 1998. How the thermospheric circulation affects the ionospheric F2-layer. J. Atmos. Solar-Terr. Phys. 60, 1385–1402.
Rodger, A.S., Moffett, R.J., Quegan, S., 1992. The role of ion drift in the formation of ionisation troughs in the mid- and high-latitude ionosphere – a review. J. Atmos. Terr. Phys. 54, 1–30. https://doi.org/10.1016/0021-9169(92)90082-V.
Seaton, M.J., 1956. A possible explanation of the drop in F-region critical densities accompanying major ionospheric storms. J. Atmos. Terr. Phys. 8, 122.
Shpynev, B.G., Zolotukhina, N.A., Polekh, N.M., Ratovsky, K.G., Chernigovskaya, M.A., Belinskaya, A.Yu, et al., 2018. The ionosphere response to severe geomagnetic storm in March 2015 on the base of the data from Eurasian high-middle latitudes ionosonde chain. J. Atmos. Solar-Terr. Phys. 180, 93–105. https://doi.org/10.1016/j.jastp.2017.10.014.
Singh, R., Scipión, D.E., Kuyeng, K., et al., 2024. Ionospheric disturbances observed over the Peruvian sector during the Mother's Day Storm (G5-level) on 10–12 May 2024. J. Geophys. Res. Space Phys. 129, e2024JA033003. https://doi.org/10.1029/2024JA033003.
Spogli, L., Alberti, T., Bagiacchi, P., et al., 2024. The effects of the May 2024 Mother's Day superstorm over the Mediterranean sector: from data to public communication. Ann. Geophys. 67 (2), PA218. https://doi.org/10.4401/ag-9117.
Sugiura M., Kamei T., 1991. Equatorial Dst index 1957–1986 // IAGA bull., 40. Saint. Maur-des-Fosses, France: ISGI (International Service Geomagnetic Indices) Publication Office.
SWPC PRF 2541, 13 May 2024 – The NOAA SWPC (Space Weather Prediction Center) PRF (Preliminary Report and Forecast) 2541 issued on 13 May 2024. ftp://ftp.swpc.noaa.gov/pub/warehouse.
Themens, D.R., Elvidge, S., McCaffrey, A., et al., 2024. The high latitude ionospheric response to the major May 2024 geomagnetic storm: a synoptic view. Geophys. Res. Lett. 51 (19), e2024GL111677. https://doi.org/10.1029/2024GL111677.
Troshichev, O.A., Sormakov, D.A., 2018. PC index as a proxy of the solar wind energy that entered into the magnetosphere: 3. Development of magnetic storms. J. Atmos. Solar-Terr Phys. 180. https://doi.org/10.1016/j.jastp.2017.10.012.
Tsurutani, B., Mannucci, A., Iijima, B., Abdu, M.A., Sobral, J.H.A., Gonzalez, W., et al., 2004. Global dayside ionospheric uplift and enhancement associated with interplanetary electric fields. J. Geophys. Res. 109, A08302. https://doi.org/10.1029/2003JA010342.
Tulasi, R.S., Veenadhari, B., Dimri, A.P., et al., 2024. Super-intense geomagnetic storm on 10–11 May 2024: possible mechanisms and impacts. Space Weather. 22 (12), e2024SW004126. https://doi.org/10.1029/2024SW004126.
Uma, G., Brahmanandam, P.S., Kakinami, Y., Dmitriev, A., Latha Devi, N.S.M.P., Uday, K.K., Prasad, D.S.V.V.D., Rama Rao, P.V.S., Niranjan, K., Seshu Babu, Ch., Chu, Y.H., 2012. Ionospheric responses to two large geomagnetic storms over Japanese and Indian longitude sectors. J. Atmos. Solar-Terr Phys. 74, 94–110. https://doi.org/10.1016/j.jastp.2011.10.001.
Vystavnoi, V.M., Makarova, L.N., Shirochkov, A.V., Egorova, L.V., 2013. Issledovaniya vysokoshirotnoi ionosfery metodom vertikal'nogo zondirovaniya s ispol'zovaniem sovremennogo tsifrovogo ionozonda CADI (Research of the high-latitude ionosphere by vertical sounding using a modern digital ionosonde CADI). Geliogeofizicheskie Issledovaniya. 4, 1–10 (in Russian).
Yasyukevich, Y.V., Vasiliev, R.V., Rubtsov, A.V., et al., 2025. Extreme magnetic storm of May 10–19, 2024: coupling between neutral and charged components of the upper atmosphere and the effect on radio systems. Doklady Earth Sci. 520. https://doi.org/10.1134/S1028334X24604978.